



# Targeted truncation of the ADAM17 cytoplasmic domain in mice results in protein destabilization and a hypomorphic phenotype

Received for publication, November 22, 2020, and in revised form, April 21, 2021. Published, Papers in Press, May 4, 2021.

<https://doi.org/10.1016/j.jbc.2021.100733>

Jose Lora<sup>1,2</sup>, Gisela Weskamp<sup>2</sup>, Thomas M. Li<sup>3</sup> , Thorsten Maretzky<sup>4</sup>, Dorjee T. N. Shola<sup>5</sup> , Sébastien Monette<sup>6</sup>, Stefan F. Lichtenthaler<sup>7,8,9,10</sup>, Theresa T. Lu<sup>3,11</sup>, Chingwen Yang<sup>5</sup>, and Carl P. Blobel<sup>1,2,10,12,13,\*</sup>

From the <sup>1</sup>Physiology, Biophysics and Systems Biology Program, Weill Cornell Medicine, New York, New York, USA; <sup>2</sup>Arthritis and Tissue Degeneration Program, <sup>3</sup>Autoimmunity and Inflammation Program, Hospital for Special Surgery, New York, New York, USA; <sup>4</sup>Inflammation Program and Department of Internal Medicine, Roy J. and Lucille A. Carver College of Medicine, University of Iowa, Iowa City, Iowa, USA; <sup>5</sup>CRISPR and Genome Editing Resource Center, Rockefeller University, New York, New York, USA; <sup>6</sup>Tri-Institutional Laboratory of Comparative Pathology, Sloan-Kettering Institute, New York, New York, USA; <sup>7</sup>German Center for Neurodegenerative Diseases (DZNE), Technical University of Munich, Munich, Germany; <sup>8</sup>Neuroproteomics, School of Medicine, Klinikum rechts der Isar, Technical University of Munich, Munich, Germany; <sup>9</sup>Munich Cluster for Systems Neurology (SyNergy), Technical University of Munich, Munich, Germany; <sup>10</sup>Institute for Advanced Study, Technical University of Munich, Garching, Germany; <sup>11</sup>Department of Microbiology and Immunology, <sup>12</sup>Department of Medicine, <sup>13</sup>Department of Biophysics, Physiology and Systems Biology, Weill Cornell Medicine, New York, New York, USA

Edited by Qi-Qun Tang

A disintegrin and metalloprotease 17 (ADAM17) is a cell-surface metalloprotease that serves as the principle sheddase for tumor necrosis factor  $\alpha$  (TNF $\alpha$ ), interleukin-6 receptor (IL-6R), and several ligands of the epidermal growth factor receptor (EGFR), regulating these crucial signaling pathways. ADAM17 activation requires its transmembrane domain, but not its cytoplasmic domain, and little is known about the role of this domain *in vivo*. To investigate, we used CRISPR-Cas9 to mutate the endogenous *Adam17* locus in mice to produce a mutant ADAM17 lacking its cytoplasmic domain (*Adam17 $\Delta$ cyto*). Homozygous *Adam17 $\Delta$ cyto* animals were born at a Mendelian ratio and survived into adulthood with slightly wavy hair and curled whiskers, consistent with defects in ADAM17/EGFR signaling. At birth, *Adam17 $\Delta$ cyto* mice resembled *Adam17*<sup>-/-</sup> mice in that they had open eyes and enlarged semilunar heart valves, but they did not have bone growth plate defects. The deletion of the cytoplasmic domain resulted in strongly decreased ADAM17 protein levels in all tissues and cells examined, providing a likely cause for the hypomorphic phenotype. In functional assays, *Adam17 $\Delta$ cyto* mouse embryonic fibroblasts and bone-marrow-derived macrophages had strongly reduced ADAM17 activity, consistent with the reduced protein levels. Nevertheless, ADAM17 $\Delta$ cyto could be stimulated by PMA, a well-characterized posttranslational activator of ADAM17, corroborating that the cytoplasmic domain of endogenous ADAM17 is not required for its rapid response to PMA. Taken together, these results provide the first evidence that the cytoplasmic domain of ADAM17 plays a pivotal role *in vivo* in regulating ADAM17 levels and function.

Cell-cell interactions are crucial for the development and maintenance of multicellular organisms. Protein ectodomain shedding of membrane-anchored signaling molecules and their receptors is considered an important mechanism for regulating cell-cell communications (1–4). A disintegrin and metalloprotease 17 (ADAM17, A17, also referred as tumor necrosis factor  $\alpha$  (TNF $\alpha$ ) converting enzyme or TACE) was first discovered as the cell-surface metalloprotease that releases TNF $\alpha$  from its membrane anchor to elicit proinflammatory responses (5, 6). In addition, ADAM17 is the principal physiological sheddase for several ligands of the epidermal growth factor receptor (EGFR) (3, 7–9), the interleukin-6 receptor (IL-6R) (10, 11), and other cytokines and receptors (1–4). ADAM17 controls EGFR signaling during development (7, 9, 12–15) and has a key role in maintaining the skin and intestinal barrier (16–18). However, ADAM17 can also contribute to the pathogenesis of EGFR-dependent cancers (1, 19, 20), pathological neovascularization (21), and the development of autoimmune diseases involving dysregulated TNF $\alpha$  release and IL-6 trans-signaling *via* the soluble IL-6R (10, 11, 22, 23).

ADAM17 can be rapidly and posttranslationally activated in response to various physiological stimuli and to treatment with the phorbol ester phorbol 12-myristate 13-acetate (PMA) in a mechanism that requires its transmembrane domain, but not its cytoplasmic domain (24–28). The transmembrane domain of ADAM17 interacts with the seven-membrane-spanning inactive Rhomboid proteins 1 and 2 (iRhom1 and 2), which are crucial for the maturation and function of ADAM17 (29–32). The cytoplasmic domain of ADAM17 contains protein-protein interaction domains, phosphorylation sites, and signaling motifs that have been suggested to play important roles in its function, regulation, subcellular transport, and

\* For correspondence: Carl P. Blobel, [blobelc@hss.edu](mailto:blobelc@hss.edu).

## ADAM17 levels depend on its cytoplasmic domain in mice

recycling (33–43). However, the functional significance of the cytoplasmic domain of ADAM17 *in vivo* has remained elusive. The goal of this study was to generate mice carrying a mutant form of endogenous ADAM17 that lacks its cytoplasmic domain, including all previously described signaling motifs, in order to learn more about the role of the cytoplasmic domain in regulating the function of ADAM17 *in vivo*.

### Results

#### Generation and characterization of Adam17 $\Delta$ cyto mice

In order to generate mice that express endogenous ADAM17 with a truncated cytoplasmic domain, we used CRISPR-Cas9 to introduce a targeted knock-in (KI) mutation, in which an HA-tag with a stop codon was attached immediately C-terminal to the transmembrane domain of ADAM17 (following DKKLD<sup>699</sup>, Fig. 1A, see [Experimental procedures](#) and [Fig. S1](#) for details). The resulting mutant ADAM17 $\Delta$ cyto lacks almost all of the cytoplasmic domain of ADAM17

(cytoplasmic amino acid residues 700–827) and corresponds to an ADAM17 $\Delta$ cyto mutant that fully rescues ADAM17-dependent shedding when overexpressed in *Adam17*<sup>-/-</sup> mouse embryonic fibroblasts (mEFs) (27). Founder mice carrying the *Adam17* $\Delta$ cyto KI mutation were generated following standard protocols (see [Experimental procedures](#) for details) and bred to homozygosity. The presence of the *Adam17* $\Delta$ cyto mutation was verified by sequencing PCR fragments from genomic DNA of mutant mice compared with *wild-type* controls (Fig. 1, B and C). Offspring of heterozygous matings (*Adam17* $\Delta$ cyto/+  $\times$  *Adam17* $\Delta$ cyto/+) were genotyped by genomic PCR (Fig. 1D) and were born at the expected Mendelian ratio (Fig. 1E).

Homozygous mutant *Adam17* $\Delta$ cyto animals appeared grossly normal (Fig. 2A) and did not display behavioral abnormalities during routine handling compared with *wild-type* controls. However, closer inspection revealed that *Adam17* $\Delta$ cyto mice had slightly wavy fur (Fig. 2B) and curly whiskers (Fig. 2C, red arrows), which are characteristic phenotypes for

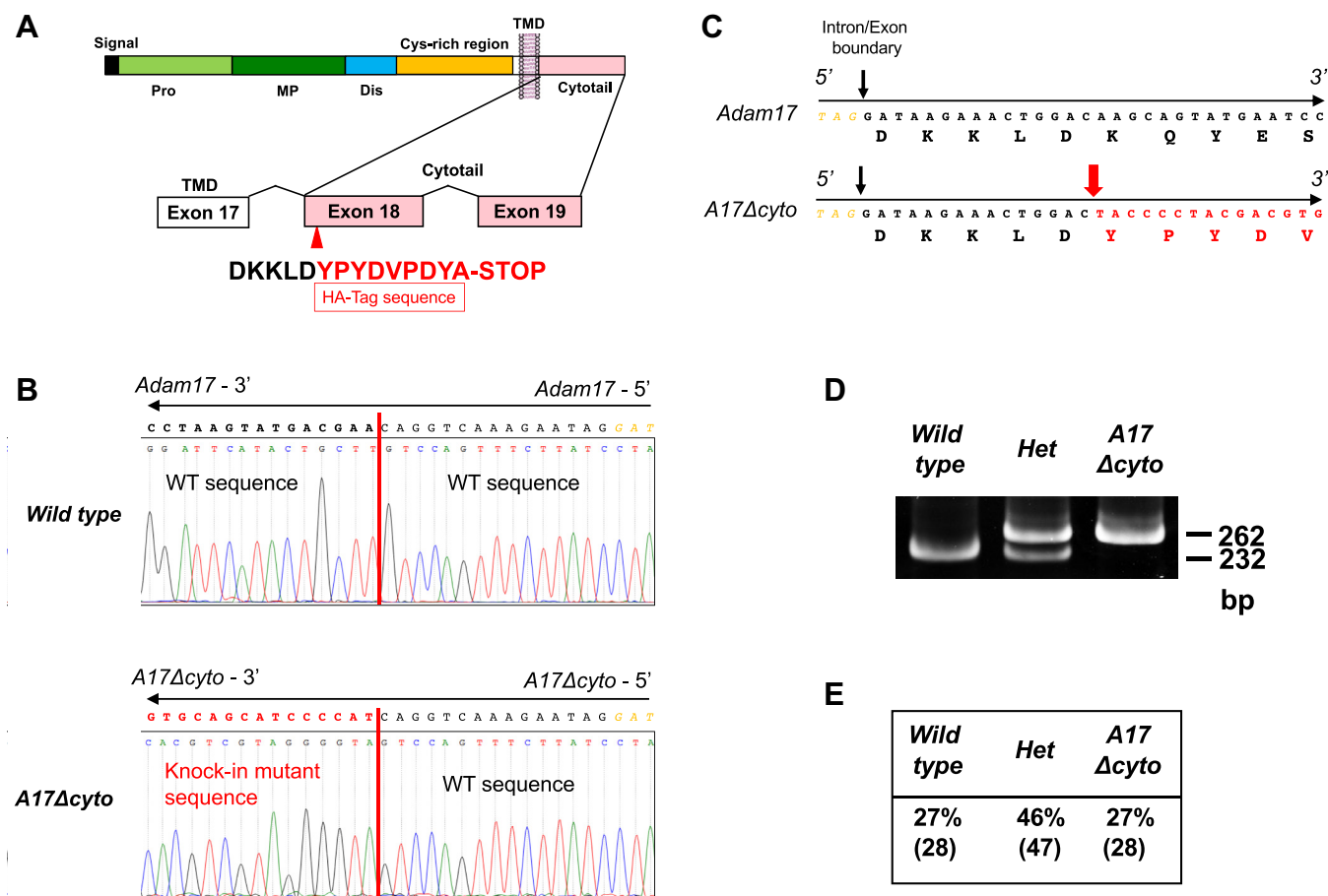


**Figure 1. Generation of Adam17 $\Delta$ cyto mice and Mendelian distribution of offspring.** A, diagram of the domain organization of ADAM17 (top) and of the corresponding transmembrane and cytoplasmic domain exons (bottom). A sequence coding for an HA-tag followed by a stop codon (red capital letters) was knocked-in adjacent to the cytoplasmic boundary of the transmembrane domain after the sequence DKKLD (black capital letters). B, genomic DNA sequence traces of the antisense strand of the targeted sequence in *Adam17* $\Delta$ cyto mice and the corresponding *wild-type* sequence. The coding sequence is shown above the trace sequence going 5'  $\rightarrow$  3' from right to left, starting from the intergenic triplet TAG-5' in black downstream of the intron/exon boundary in yellow. The position of the targeted insertion site is indicated by a vertical red line, with the knock-in mutant sequence shown in red capital letters above the *Adam17* $\Delta$ cyto sequence traces (bottom panel). C, the resulting genomic sequence of the *wild-type* locus or the targeted locus in *Adam17* $\Delta$ cyto mice is shown in 5'  $\rightarrow$  3' orientation from left to right with the amino acid sequence translated from the coding region. D, PCR genotyping results generated from *wild-type*, *Adam17* $\Delta$ cyto heterozygotes, and *Adam17* $\Delta$ cyto homozygotic mutants. E, offspring from *Adam17* $\Delta$ cyto het  $\times$  het matings were born at an approximately Mendelian ratio.

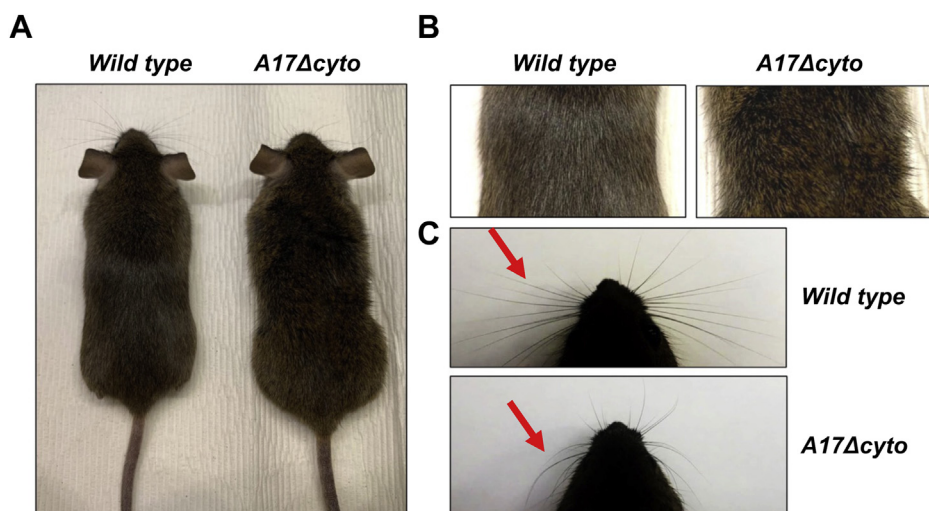


**Figure 2. Adult *Adam17Δcyto* mice have wavy fur and curly whiskers.** A, representative images of 6-month-old *wild-type* and *Adam17Δcyto* littermates show a wavy fur phenotype in the *Adam17Δcyto* mouse compared with the *wild-type* control. An enlarged image of the wavy fur in an adult *Adam17Δcyto* mouse is shown together with a *wild-type* control in (B). The curly whiskers in a 3-week-old mutant mouse are shown in comparison to straight whiskers in an age-matched *wild-type* mouse in (C). All images are representative samples for typical *wild-type* or *Adam17Δcyto* mice.

mice carrying mutations affecting ADAM17/EGFR signaling (16, 44, 45).

Gross and histopathological analysis of newborn mice revealed that *Adam17Δcyto* animals resemble *Adam17<sup>-/-</sup>* animals in that their eyes are open at birth (Fig. 3A, top two rows of panels) (7, 46). Moreover, *Adam17Δcyto* mice show enlarged and thickened pulmonic, aortic, and tricuspid heart valves (Fig. 3A, middle and lower middle panels, tricuspid valve not shown), similar to *Adam17<sup>-/-</sup>* mice (12, 46). However, unlike *Adam17<sup>-/-</sup>* mice (14, 15), *Adam17Δcyto* mice did not have significantly expanded zones of hypertrophic cells in their long bone growth plate (Fig. 3A, femur shown in lower panel).

Analysis of adult *Adam17Δcyto* animals showed no evident abnormalities in heart weight and gross and histologic morphology of the heart, including the heart valves (Fig. 3B, left panels), suggesting that the heart valve defects are remodeled and return to normal as these animals grow into adults. In addition, we found pyogranulomatous inflammation of hair follicles in the skin and in the meibomian glands in eyelids and zymbal glands near the ear canal, which are both specialized sebaceous glands (Fig. 3B, right panels). There were no other major evident pathological phenotypes in the adult *Adam17Δcyto* mice compared with their littermate controls.

#### Strong reduction in ADAM17 protein levels in *Adam17Δcyto* mouse embryonic fibroblasts

The hypomorphic phenotype of *Adam17Δcyto* mice raised questions about the underlying cause for the apparently reduced activity of ADAM17. We therefore performed western blots on Concanavalin A-enriched glycoproteins isolated from *wild-type*, *Adam17Δcyto*, and *Adam17<sup>-/-</sup>* mEFs with rabbit polyclonal antibodies raised against the extracellular domain of mouse ADAM17 (anti-A17-ecto). The samples were run under denaturing, but nonreducing conditions, since the anti-A17-ecto antibodies only recognize nonreduced ADAM17 in western blots (see Fig. S2 and Experimental procedures for

details). Under these conditions, the anti-A17-ecto antibody detected the wild-type proform of ADAM17 (Fig. 4A, indicated by an open arrowhead) as well as the mature form (indicated by a black arrowhead) in mEFs. By comparison, the levels of pro-ADAM17Δcyto (open arrowhead) and mature ADAM17Δcyto (black arrowhead) were strongly reduced. When *wild-type* cells were lysed in the absence of metalloprotease inhibitors (marimastat and 1,10 Phenanthroline, see Experimental procedures for details), the mature form of wild-type ADAM17 underwent postlysis autocatalytic removal of the cytoplasmic domain, as reported previously (47, 48), which generates a faster migrating form of mature ADAM17 (Fig. 4A, indicated by an asterisk), whereas pro-ADAM17 was not affected. A similar postlysis autocatalytic removal of the cytoplasmic domain was also observed in the related ADAM10 and is thought to have no biological significance in ADAM17 or ADAM10 (49). The proform of ADAM17Δcyto (open arrowhead in Fig. 4A, darker exposure shown on the right) migrated faster than the proform of wild-type ADAM17, consistent with the predicted reduction in molecular weight caused by deletion of the cytoplasmic domain. The mature form of ADAM17Δcyto (black arrowhead in Fig. 4A) comigrated approximately with the autodegraded form of mature wild-type ADAM17 (asterisk). However, the presence or absence of the metalloprotease inhibitors during cell lysis did not affect the migration of mature ADAM17Δcyto. This suggests that ADAM17Δcyto was not detectably subjected to postlysis processing, presumably because it lacks the cytoplasmic domain that is removed by this process in wild-type ADAM17. The samples from *Adam17<sup>-/-</sup>* mEFs served as negative control for the selectivity of the anti-A17-ecto antibodies.

Cell surface biotinylation followed by western blot analysis of streptavidin-purified biotinylated proteins showed that only the mature forms of wild-type ADAM17 and of ADAM17Δcyto (black arrowheads) were present at the cell surface (Fig. 4B, darker exposure for ADAM17Δcyto shown in the

## ADAM17 levels depend on its cytoplasmic domain in mice

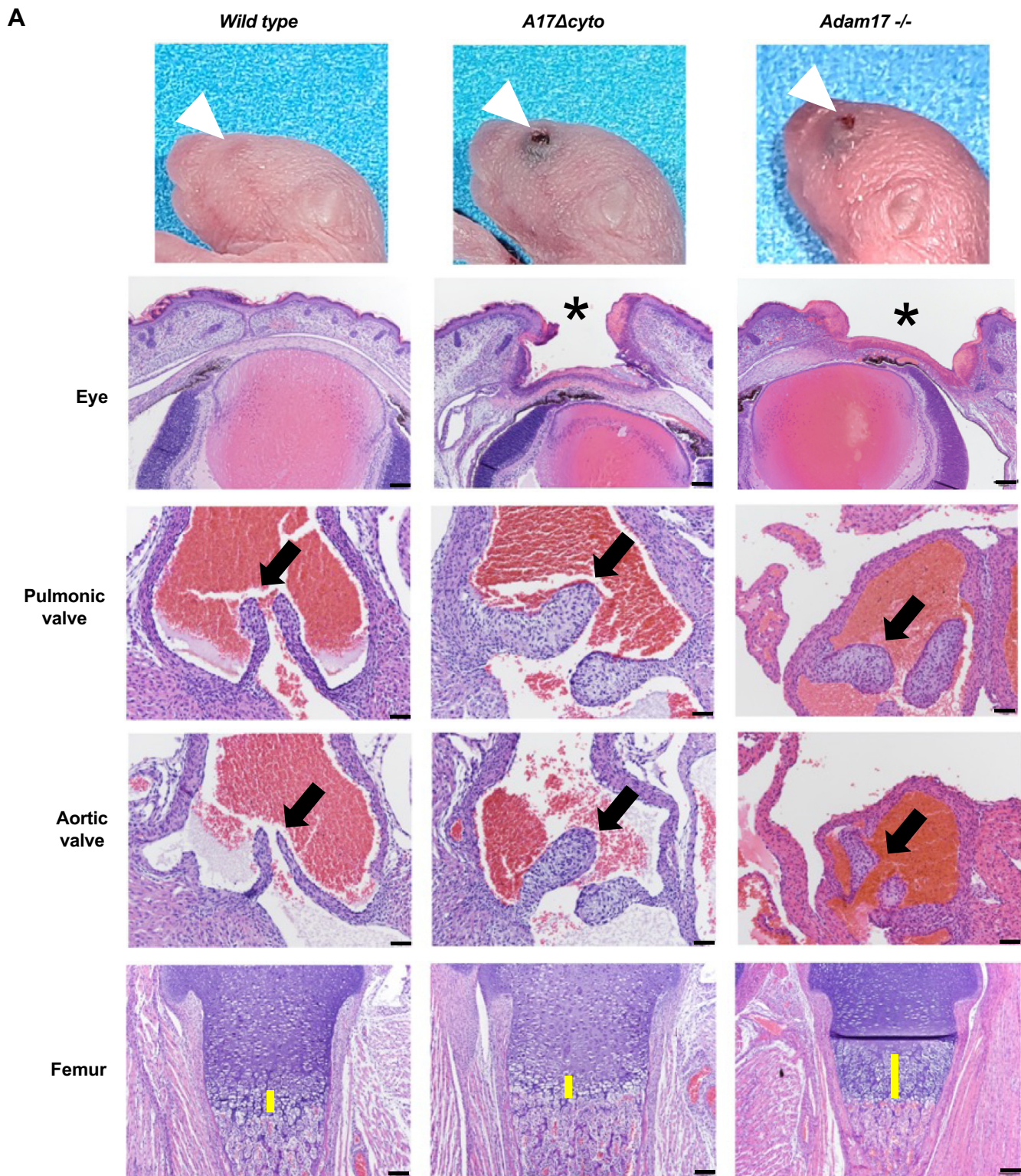


**Figure 3. *Adam17 $\Delta$ cyto* mice closely resemble *Adam17<sup>-/-</sup>* mice at birth.** A, representative images of the heads of newborn *wild-type* and *Adam17 $\Delta$ cyto* (littermates) and *Adam17<sup>-/-</sup>* mice show open eyes at birth (OEB) in *Adam17 $\Delta$ cyto* mutants that are similar to the OEB in *Adam17<sup>-/-</sup>* mice (top row, white arrows). Corresponding H&E-stained sections of the eye are shown in row 2, with an asterisk marking the open eyelid. Sections of a representative pulmonic valve (middle panel/row 3) and aortic valve (row 4) show similarly enlarged and misshapen tricuspid valves in *Adam17 $\Delta$ cyto* mutants compared with *Adam17<sup>-/-</sup>* mice. However, the growth plate in the *Adam17 $\Delta$ cyto* mutant appeared normal in size and comparable to the *wild-type* control and did not display the enlarged zone of hypertrophic cells seen in *Adam17<sup>-/-</sup>* mice (bottom row). Scale bars: sections of eyes and femurs, 100  $\mu$ m, sections of heart valves, 50  $\mu$ m. B, representative images of the aortic and pulmonic valves in adult *Adam17 $\Delta$ cyto* mutants are indistinguishable from *wild-type* controls (left panels). The hair follicles and skin of *Adam17 $\Delta$ cyto* mutants showed pyogranulomatous inflammation, which also affected the meibomian glands in the eyelids and the zymbal glands near the ear canal (Fig. 3B, right panels). Scale bars: sections of adult heart valves, 100  $\mu$ m, sections of skin and glands, 50  $\mu$ m. All images are representative for sections from at least three mice per genotype.

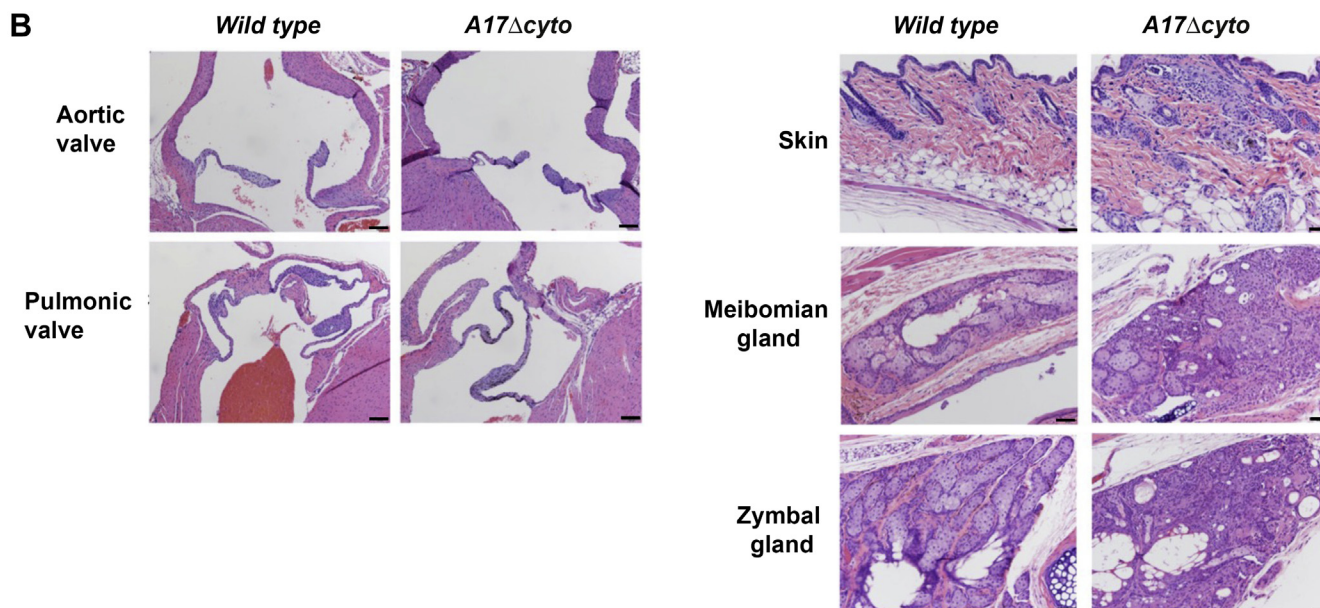


Figure 3. (Continued).

right panel). A densitometric comparison of cell surface biotinylated mature ADAM17 to the total ADAM17 detected by western blot showed a similar ratio for the wild-type and ADAM17 $\Delta$ cyto proteins (ratio of biotinylated ADAM17 to total ADAM17, wild-type average 0.46 arbitrary units, SEM 0.013; ADAM17 $\Delta$ cyto average 0.49 arbitrary units, SEM 0.094, Student's *t*-test *p*-value 0.78, see [Experimental procedures](#) for details). Taken together, these results demonstrated that the deletion of the cytoplasmic domain of endogenous ADAM17 affects its levels in mEFs, but that the ADAM17 $\Delta$ cyto protein is nevertheless processed in the secretory pathway and transported to the cell surface.

Previous studies have shown that the presence of ADAM17 stabilizes its regulatory binding partner iRhom2, but not iRhom1 (50). Consistent with this observation, we found very low levels of iRhom2 in ADAM17 $\Delta$ cyto mEFs, similar to ADAM17 $^{-/-}$  mEFs (Fig. 4D). The levels of iRhom1 appeared slightly increased in ADAM17 $\Delta$ cyto mEFs, just like those observed in ADAM17 $^{-/-}$  mEFs (50). These findings further corroborate the dependence of iRhom2, but not iRhom1 on the levels of ADAM17.

#### Strongly reduced ADAM17 protein levels in ADAM17 $\Delta$ cyto mouse tissues

As a next step, we performed western blots with anti-A17-ecto on extracts from the brain, heart, lung, liver, and spleen tissue of wild-type and ADAM17 $\Delta$ cyto mice. This corroborated that the levels of both pro- and mature ADAM17 were strongly reduced in these tissues in ADAM17 $\Delta$ cyto mice compared with controls (Fig. 5A, black arrowhead indicates mature wild-type ADAM17, or ADAM17 $\Delta$ cyto, the proform of ADAM17 is not detected efficiently by the anti-A17-ecto antibodies in tissues, please see Fig. S2 for details). In some cases, the wild-type samples contained a small amount of the autodegraded mature form of ADAM17 (asterisk in Fig. 5A

(47, 48)). An analysis of the mRNA levels of wild-type or mutant ADAM17 by qPCR in the lung and liver showed an upward, but not significant trend in mRNA levels, whereas there was a significant increase in the expression of ADAM17 mRNA in ADAM17 $\Delta$ cyto brain, heart, and spleen compared to wild-type controls (Fig. 5B). When we performed flow cytometry analysis of skin cells that were positive for the epithelial cell adhesion molecule (EPCAM<sup>+</sup>, mostly keratinocytes), we saw a strong reduction in surface ADAM17 signal in cells from ADAM17 $\Delta$ cyto mice compared with wild-type controls (Fig. 6, A and B). Taken together, these findings emphasize that the truncation of the cytoplasmic domain of endogenous ADAM17 strongly affects the levels of ADAM17 $\Delta$ cyto in different tissues and cells in mice, most likely in a posttranslational manner.

#### Activity of ADAM17 $\Delta$ cyto in mEFs

Next, we tested how the substantially reduced levels of ADAM17 $\Delta$ cyto in ADAM17 $\Delta$ cyto mEFs affected the shedding of the ADAM17-substrate TGF $\alpha$ . We found that PMA-stimulated processing of TGF $\alpha$  was strongly reduced in ADAM17 $\Delta$ cyto mEFs compared with wild-type controls (Fig. 7A), presumably caused by the strong decrease in ADAM17 $\Delta$ cyto protein levels (see Fig. 4). Nevertheless, the shedding of TGF $\alpha$  was significantly enhanced by addition of the phorbol ester phorbol 12-myristate 13-acetate (PMA) in ADAM17 $\Delta$ cyto mEFs (Fig. 7A), although the fold increase in shedding upon addition of PMA was reduced. Specifically, the PMA-stimulated increase in TGF $\alpha$  shedding in wild-type mEFs was on average 3.37-fold over the shedding levels in untreated controls (SEM 0.34), whereas ADAM17 $\Delta$ cyto mEFs showed an average of 1.86-fold increase upon PMA stimulation (SEM 0.28). These results are consistent with previous studies that used overexpressed ADAM17 $\Delta$ cyto in that the cytoplasmic domain of endogenous ADAM17 is not required for its rapid

## ADAM17 levels depend on its cytoplasmic domain in mice

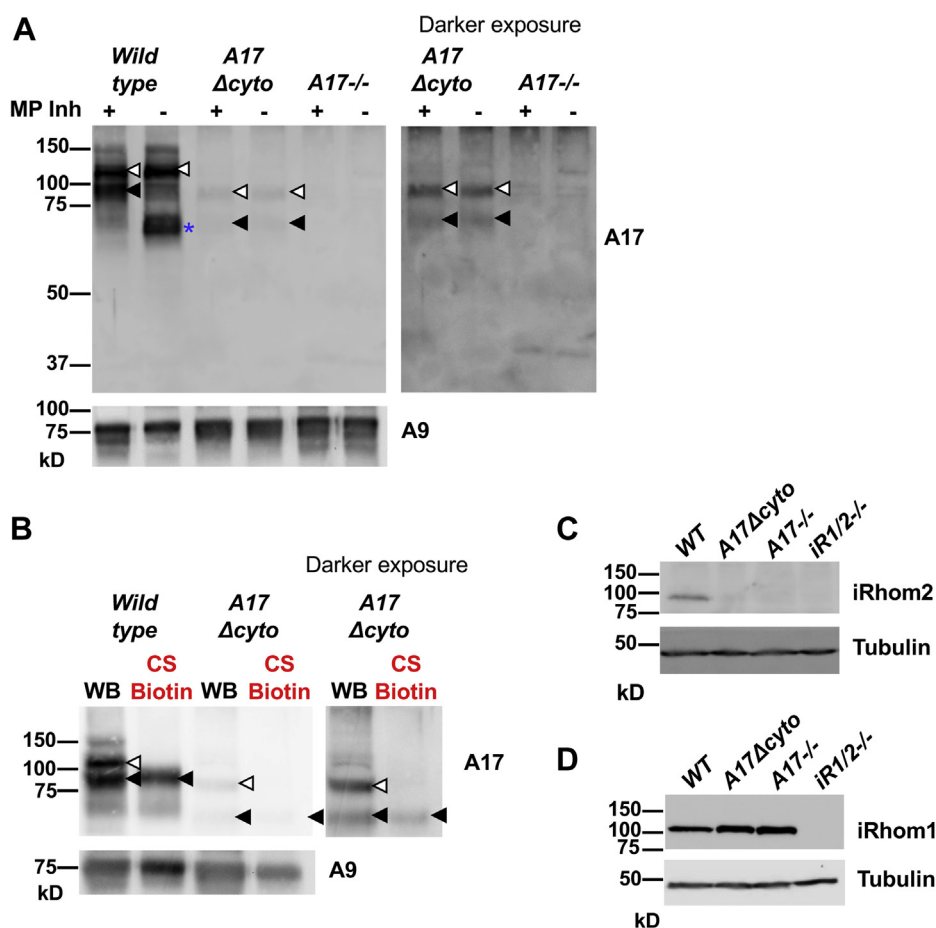


**Figure 4. Strongly reduced levels of endogenous ADAM17 $\Delta$ cyto protein in mouse embryonic fibroblasts.** *A*, mouse embryonic fibroblasts (mEFs) were lysed in the presence or absence of the metalloprotease (MP) inhibitors marimastat (5  $\mu$ m) and 1,10 Phenanthroline (10 mM), as indicated. Concanavalin A-enriched glycoproteins were subjected to a western blot analysis with anti-ADAM17-ecto antibodies, which showed strongly reduced expression of endogenous ADAM17 $\Delta$ cyto protein compared with wild-type ADAM17, with samples from *Adam17* $^{-/-}$  mEFs serving as negative control for the selectivity of the antibodies and ADAM9 (A9) as a loading control. The *right panel* shows a longer exposure of the *Adam17* $\Delta$ cyto and *Adam17* $^{-/-}$  samples to better visualize the pro- and mature forms of ADAM17 $\Delta$ cyto. The postlysis autocatalytic degradation of mature wild-type ADAM17 in the absence of metalloprotease (MP) inhibitors can be seen in lane 2 of the wild-type sample (47, 48). *B*, western blot analysis (WB) compared with cell surface Biotin labeling (CS biotin) of ADAM17 and ADAM17 $\Delta$ cyto (see [Experimental procedures](#) for details). An *open arrowhead* indicates the proform, and a *black arrowhead* indicates the mature form of endogenous wild-type ADAM17 or ADAM17 $\Delta$ cyto. *C* and *D*, whole-cell lysates of *wild-type*, *Adam17* $\Delta$ cyto, *Adam17* $^{-/-}$ , and *iRhom1/2* $^{-/-}$  mEFs were subjected to western blot analysis using monoclonal rat-antibodies against iRhom2 (*C*, *top panel*) or iRhom1 (*D*, *top panel*) or antibodies against alpha-tubulin (*lower panels* in *C* and *D*) as a loading control. The levels of iRhom2 were strongly reduced in *Adam17* $\Delta$ cyto, just like in *Adam17* $^{-/-}$  mEFs, whereas the iRhom1 levels were slightly increased in *Adam17* $\Delta$ cyto mEFs, as in *Adam17* $^{-/-}$  mEFs (50). Western blots for tubulin served as loading control, and lysates of *iRhom1/2* $^{-/-}$  mEFs served as reagent controls for the selectivity of the rat anti-iRhom1 or iRhom2 monoclonal antibodies. Each experiment was repeated three times with essentially similar results and one representative blot is shown.

activation following PMA stimulation (27), although the fold increase is lower than that for wild-type ADAM17. The strong reduction in shedding in the *Adam17* $\Delta$ cyto mEFs was also reflected in the increased levels of presumably unprocessed TGF $\alpha$ -AP in the cell lysates, which were similar to the levels in *Adam17* $^{-/-}$  mEFs (Fig. 7B).

### Characterization of ADAM17 $\Delta$ cyto levels and function in bone-marrow-derived macrophages (BMDMs)

Previous studies have shown that the function of ADAM17 depends on iRhom2 in cells of myeloid origin, raising questions about how the truncation of the ADAM17 cytoplasmic domain impacts its levels and activity in these cells. We found strongly reduced levels of pro and mature ADAM17 $\Delta$ cyto in bone-marrow-derived macrophages (BMDMs) from *Adam17* $\Delta$ cyto mice compared with controls (Fig. 8A),

consistent with the reduction of ADAM17 $\Delta$ cyto protein levels observed in mEFs and adult tissues. A qPCR analysis showed that the mRNA levels for *Adam17* $\Delta$ cyto are slightly but significantly higher than the mRNA levels for *Adam17* in *wild-type* BMDMs (Fig. 8B). We also found that iRhom2 cannot be detected in *Adam17* $\Delta$ cyto BMDMs under conditions where it is easily detected in *wild-type* controls (Fig. 8C), just as in mEFs (see above), with *iRhom2* $^{-/-}$  BMDMs serving as control for the specificity of the anti-iRhom2 antibodies.

To measure ADAM17-dependent shedding of an endogenous substrate in *Adam17* $\Delta$ cyto BMDMs, we monitored the cell surface levels of colony stimulating factor 1 receptor (Csf1r) *via* flow cytometry (51–53). Stimulation of BMDMs with PMA triggered a strong reduction in cell surface Csf1r levels in *wild type* and in *Adam17* $\Delta$ cyto BMDMs compared with untreated controls (Fig. 9, A and B), although the shift

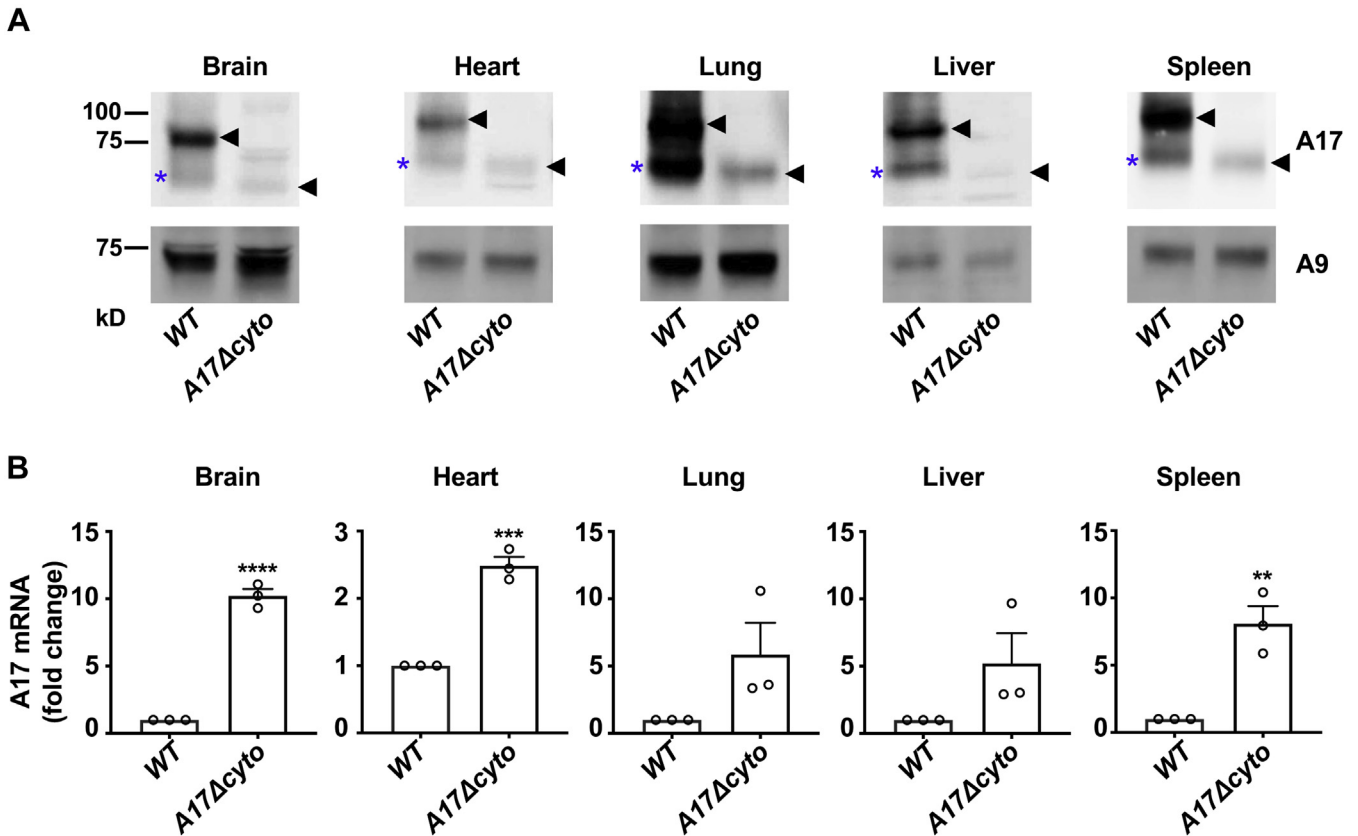


**Figure 5. Reduced levels of ADAM17Δcyto protein but not mRNA in selected tissues of adult *Adam17Δcyto* mice.** *A*, representative western blots of extracts from the brain, heart, lung, liver, and spleen of adult mice show a strong reduction in ADAM17Δcyto protein levels compared with wild-type controls. *B*, *Adam17* mRNA expression in the brain, heart, lung, liver, and spleen of adult *wild-type* and *Adam17Δcyto* mice ( $n = 3$ , Student's *t*-test, \* indicates a *p*-value of <0.05). Each western blot is representative for at least three separately prepared western blots, each from mice from a different litter. *Black arrowhead*, mature wild-type or ADAM17Δcyto, as indicated, *blue asterisk*, postlysis autodegradation artifact of mature wild-type ADAM17. Western blots for ADAM9 are shown as loading control.

was weaker in the *Adam17Δcyto* cells. There was only a slight drop in Csf1r levels in PMA-treated *iRhom2*<sup>-/-</sup> BMDMs compared with untreated controls, as described previously

(Fig. 9C) (52). In nonstimulated cells, the surface levels of Csf1r were slightly lower in *Adam17Δcyto* BMDMs compared with *iRhom2*<sup>-/-</sup> BMDMs, which have no detectable mature

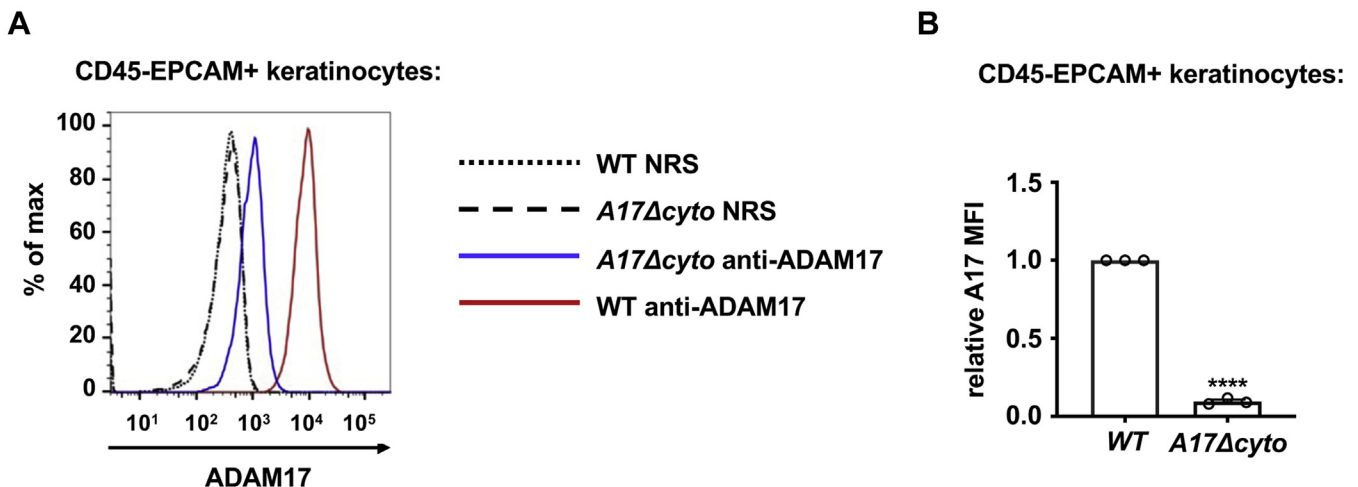


**Figure 6. Flow cytometric analysis of ADAM17 levels on the surface of cells isolated from mouse skin.** Cell surface ADAM17 levels on *ex vivo* keratinocytes. Ears from *wild-type* or *Adam17Δcyto* mice were digested to single cell suspensions, stained with anti-ADAM17 or normal rabbit serum (NRS) control along with cellular markers, and subjected to flow cytometric analysis. *A*, histograms of ADAM17 levels for live-gated CD45- EPCAM+ cells (mostly keratinocytes). *B*, mean fluorescence intensity (MFI) of ADAM17 signal normalized to the signal in the *wild-type* sample for each experiment. A representative example from three separate experiments is shown in *A*, each symbol represents one mouse in *B*. \* indicates a *p*-value of <0.05 in an unpaired Student's *t*-test.

## ADAM17 levels depend on its cytoplasmic domain in mice

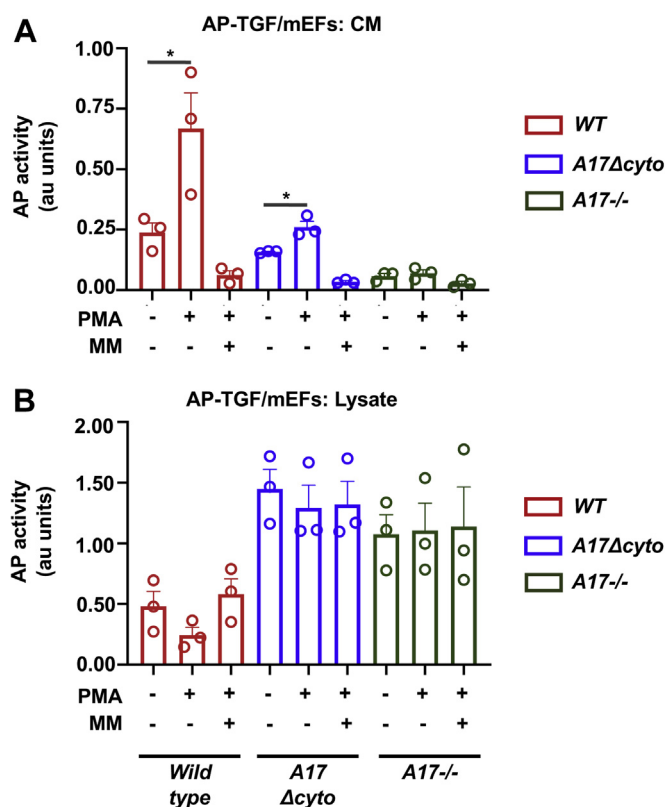


**Figure 7. *Adam17 $\Delta$ cyto* mEFs can support constitutive and PMA-stimulated shedding of the ADAM17 substrate TGF $\alpha$  at overall reduced levels.** mEFs from *wild-type*, *Adam17 $\Delta$ cyto*, and *Adam17 $^{-/-}$*  mice were transfected with the alkaline phosphatase-tagged ADAM17-selective substrate TGF $\alpha$  (TGF $\alpha$ -AP) and left untreated or stimulated with 25 ng/ml PMA for 45 min in the presence or absence of 5  $\mu$ M of the metalloprotease inhibitor marimastat. **A**, the activity of ADAM17 and ADAM17 $\Delta$ cyto is shown as the TGF $\alpha$ -AP activity in the conditioned media (CM). ADAM17 $\Delta$ cyto supports overall lower levels of TGF $\alpha$ -AP shedding, but can respond to stimulation with PMA. *Adam17 $^{-/-}$*  mEFs serve as a negative control. **B**, the reduced activity of ADAM17 $\Delta$ cyto compared with wild-type ADAM17 is also reflected in the higher levels of TGF $\alpha$ -AP in the lysates of *Adam17 $\Delta$ cyto* cells, similar to *Adam17 $^{-/-}$*  mEFs, presumably caused by the reduced overall shedding activity.  $n = 3$ . \* indicates a  $p$ -value of  $<0.05$  in an unpaired Student's  $t$ -test.

and active ADAM17 on their surface (48, 54), but substantially higher than in *wild-type* controls (Fig. 9D). These results provide independent verification that ADAM17-dependent shedding is reduced in *Adam17 $\Delta$ cyto* BMDMs, but that endogenous ADAM17 $\Delta$ cyto activity can nevertheless be enhanced by stimulation with PMA.

Since ADAM17 is the major sheddase for TNF $\alpha$  (5–7, 46), we also compared the LPS-stimulated release of TNF $\alpha$  from *wild-type*, *Adam17 $\Delta$ cyto*, and *iRhom2 $^{-/-}$*  BMDMs. We found that stimulation of *wild-type* BMDMs with LPS for 3 h resulted in strongly induced levels of TNF $\alpha$ , whereas the LPS stimulation of *Adam17 $\Delta$ cyto* BMDMs yielded a similar increase in TNF $\alpha$  shedding as in LPS-stimulated *iRhom2 $^{-/-}$*  BMDMs (Fig. 9E). Since ADAM10 is also able to cleave TNF $\alpha$  (55, 56), the similar residual TNF $\alpha$  shedding activity in *Adam17 $\Delta$ cyto* and in *iRhom2 $^{-/-}$*  BMDMs presumably depends on ADAM10, which might obscure the relatively low activity of ADAM17 $\Delta$ cyto under these conditions. However, it should

nevertheless be emphasized that ADAM17 and not ADAM10 is the principal TNF $\alpha$  convertase in the context of endotoxin shock *in vivo* (46). These results provide additional evidence for the substantial reduction of ADAM17 activity in *Adam17 $\Delta$ cyto* BMDMs compared with *wild-type* controls.

### Effect of protein translation and degradation inhibitors on ADAM17 $\Delta$ cyto levels

To explore the causes of the reduced levels of ADAM17 $\Delta$ cyto protein, we performed a cycloheximide (CHX) chase experiment in mEFs. Western blots for ADAM17 or ADAM17 $\Delta$ cyto were performed at different time points after addition of this inhibitor of protein translation (Fig. 10). Under these conditions, the levels of pro- and mature ADAM17 $\Delta$ cyto were slightly reduced compared with the wild-type control after 2 h of CHX treatment and significantly reduced after 4 h in CHX. There was no significant change in the levels of pro- or mature ADAM17 compared with the untreated cells (0 h) at any of these time points (Fig. 10B), consistent with the results of a previous pulse chase experiments with radioactively labeled wild-type ADAM17 (47).

Next, we examined whether inhibitors of lysosomal or proteasomal degradation could increase or restore the levels of ADAM17 $\Delta$ cyto in mEFs. When we incubated *Adam17 $\Delta$ cyto* mEFs with the proteasomal inhibitor MG-132 or the ER-associated degradation pathway inhibitor Eeyarestatin, no substantial changes in the levels of wild-type ADAM17 or of ADAM17 $\Delta$ cyto were detected by western blot analysis (Fig. 11A). Under these conditions, both inhibitors blocked ubiquitin degradation, which served as a control for their activity (Fig. 11A, bottom panels). Similar results were obtained when *Adam17 $\Delta$ cyto* mEFs were treated with the lysosomal degradation inhibitors chloroquine or bafilomycin, which also did not lead to a substantial increase in the levels of wild-type ADAM17 or ADAM17 $\Delta$ cyto (Fig. 10B). For both inhibitors, an increase in LC3-II served as an indicator of effective inhibition of autophagy under the conditions used here (Fig. 11B, lower panel). These results argue against a major role of lysosomal, proteasomal, or autophagosomal degradation in causing the low levels of ADAM17 $\Delta$ cyto.

### Discussion

The main goal of this study was to examine the function of the cytoplasmic domain of endogenous ADAM17 *in vivo*. Previous studies have reported that phosphorylation of the cytoplasmic domain of ADAM17 is required for its activation (40–43), whereas several other studies reported that a mutant ADAM17 lacking its cytoplasmic domain could be stimulated as well as the wild-type control (24, 26, 27). On the other hand, the maturation of overexpressed wild-type ADAM17 differed from the endogenous wild-type protein in that very little of the mature form of overexpressed ADAM17 could be detected by western blot analysis (57). The different properties of overexpressed *versus* endogenous ADAM17 provided an obstacle in the analysis of how the cytoplasmic domain controls the maturation, localization, and function of ADAM17. To

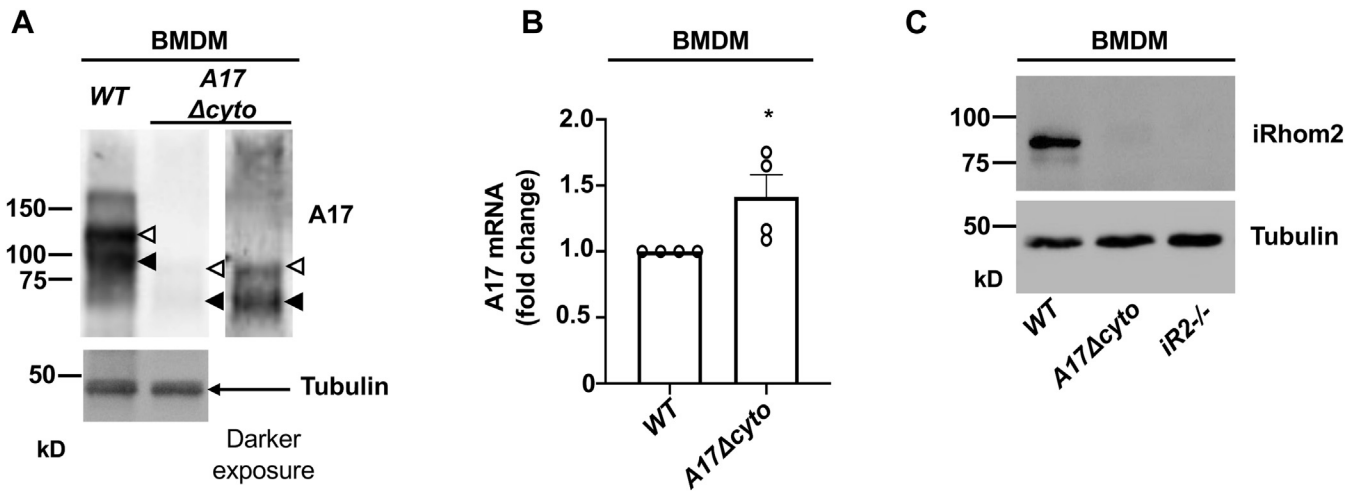


**Figure 8. Characterization of ADAM17 $\Delta$ cyto and iRhom2 expression in bone-marrow-derived macrophages (BMDMs).** A, western blots of *wild-type* and *Adam17 $\Delta$ cyto* BMDMs probed with anti-A17-ecto antibodies show strongly decreased levels of ADAM17 $\Delta$ cyto compared with wild-type ADAM17. The proform of wild-type ADAM17 or ADAM17 $\Delta$ cyto is indicated by an *open arrowhead* and the mature form of each by a *black arrowhead*. The *inset* shows a darker exposure of the ADAM17 $\Delta$ cyto lane, and anti- $\alpha$ -tubulin Westerns served as loading controls. B, a qPCR analysis showed slightly, but significantly increased expression of *Adam17 $\Delta$ cyto* mRNA compared with the *wild-type Adam17* mRNA controls. C, a Western blot for iRhom2 showed barely detectable levels in *Adam17 $\Delta$ cyto* BMDMs compared with *wild-type* controls, with *iRhom2*<sup>-/-</sup> BMDMs serving as reagent control for the anti-iRhom2 antibody, and  $\alpha$ -tubulin serving as a loading control. The western blots in panels A and C are representative of at least three separate experiments.

circumvent this problem, we used CRISPR-Cas9 to generate an endogenous ADAM17 $\Delta$ cyto mutant with the same amino acid sequence as the previously studied overexpressed ADAM17 $\Delta$ cyto (27). Here we report the analysis of the properties of the endogenously expressed ADAM17 $\Delta$ cyto in *Adam17 $\Delta$ cyto* KI mice. We show that the levels of endogenous ADAM17 $\Delta$ cyto are strongly reduced compared with wild-type controls. Nevertheless, *Adam17 $\Delta$ cyto* mice survive and are viable and fertile, although they display hypomorphic ADAM17/EGFR phenotypes with open eyes and heart valve defects at birth and curly whiskers and wavy hair as adults. The hypomorphic phenotype of *Adam17 $\Delta$ cyto* mice is most likely a consequence of the low levels of ADAM17 $\Delta$ cyto protein.

To gain a better understanding of how the decreased levels of ADAM17 $\Delta$ cyto affect its function, we performed cell-based assays for the shedding of the ADAM17 substrate TGF $\alpha$ . We found that the strong reduction in ADAM17 $\Delta$ cyto protein levels was reflected by strongly reduced activity toward TGF $\alpha$ . Nevertheless, endogenous ADAM17 $\Delta$ cyto exhibited a significant response to stimulation with the phorbol-ester PMA, a commonly used activator of ADAM17-dependent shedding of substrates such as overexpressed TGF $\alpha$  or the endogenous Csf1r (9, 52, 53), although the level of the response was reduced. Since mature ADAM17 $\Delta$ cyto and wild-type ADAM17 can be detected on the cell surface at a similar relative level compared with the total protein detectable by western blot, these findings demonstrate that ADAM17 $\Delta$ cyto can undergo maturation and is transported to the cell surface, where it can respond rapidly to PMA stimulation. Previous studies have shown that phosphorylation of iRhom2 is crucial for the iRhom2-dependent activation of ADAM17 (29–32). Moreover, several studies have shown that the stimulation of ADAM17 by iRhom2 requires sequences in the first transmembrane domain of iRhom2 and in the transmembrane

domain of ADAM17 (53, 58, 59). Taken together, these studies help explain how ADAM17 can be activated in the absence of its cytoplasmic domain *via* phosphorylation of iRhom2, which interacts with ADAM17 *via* their transmembrane domains. The functional properties of ADAM17 $\Delta$ cyto therefore corroborate previous results with overexpressed ADAM17 $\Delta$ cyto (24, 26, 27) in that the cytoplasmic domain of endogenous ADAM17 is not required for its rapid posttranslational activation by PMA.

An unexpected finding of this study was that the lack of the cytoplasmic domain of ADAM17 led to strongly reduced levels of both pro- and mature ADAM17 $\Delta$ cyto, despite normal or even increased levels of *Adam17 $\Delta$ cyto* mRNA. The strong reduction in ADAM17 $\Delta$ cyto protein levels was seen by western blot in mEFs, BMDMs, and in different tissues in adult mice and by flow cytometry in skin cells, including keratinocytes. Despite the strongly reduced levels and activity of ADAM17 $\Delta$ cyto in cell-based assays, the remaining activity was sufficient to allow *Adam17 $\Delta$ cyto* mice to survive, whereas most *Adam17*<sup>-/-</sup> mice die shortly after birth (7, 46). However, since the *Adam17 $\Delta$ cyto* mice are born with open eyes and heart valve defects, like *Adam17*<sup>-/-</sup> mice, this suggests that the normal development of these structures is sensitive to the levels and activity of ADAM17 during development. The heart valve defects were no longer apparent in adult *Adam17 $\Delta$ cyto* mice, suggesting that these defects can be repaired or remodeled after birth, although we cannot rule out that the adult animals analyzed had milder heart valve defects at birth.

The curved whiskers, wavy fur, and inflamed Meibomian glands in adult mice are consistent with a reduction in ADAM17/TGF $\alpha$ /EGFR signaling (45, 60, 61), which presumably also explains the inflammation of Zymbal glands. With respect to the curly whiskers and wavy fur, the

## ADAM17 levels depend on its cytoplasmic domain in mice

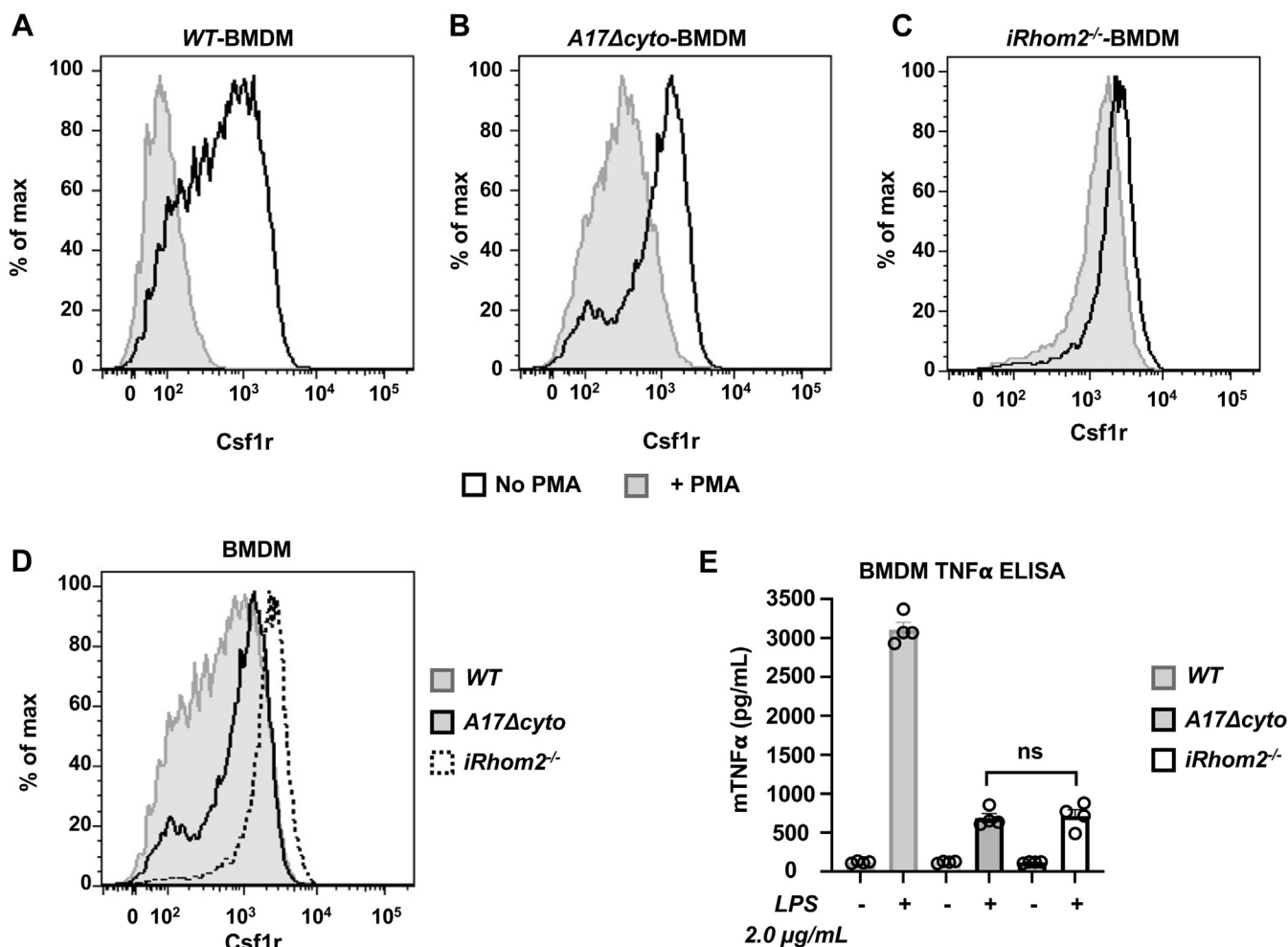


**Figure 9. Characterization of the activity of ADAM17 $\Delta$ cyto in bone-marrow-derived macrophages (BMDMs).** A–D, cell surface levels of the iRhom2/ADAM17-substrate colony stimulating 1 receptor (Csfr1) were determined by flow cytometry in *wild-type*, *Adam17 $\Delta$ cyto*, and *iRhom2<sup>-/-</sup>* BMDMs, which served as negative control because they lack functional ADAM17 at the cell surface (23, 48, 54). A–C, stimulation of BMDMs with the phorbol ester PMA (25 ng/ml for 45 min), which activates ADAM17, strongly reduced the levels of the Csfr1 on *wild-type* BMDMs (A) and led to a substantial, but somewhat weaker reduction on *Adam17 $\Delta$ cyto* BMDMs (B), with *iRhom2<sup>-/-</sup>* serving as control for the minor shift seen in the absence of ADAM17 (C). In unstimulated BMDMs, the levels of the Csfr1 were lower in *Adam17 $\Delta$ cyto* compared with *iRhom2<sup>-/-</sup>* BMDMs, but higher than in the *wild-type* controls, consistent with reduced activity in *Adam17 $\Delta$ cyto* BMDMs (D). E, a TNF $\alpha$  ELISA on the supernatants of BMDMs treated with or without 2  $\mu$ g/ml LPS for 3 h showed strongly reduced stimulation of TNF $\alpha$  production in *Adam17 $\Delta$ cyto* and *iRhom2<sup>-/-</sup>* BMDMs compared with *wild-type* controls, with no significant difference between *Adam17 $\Delta$ cyto* and *iRhom2<sup>-/-</sup>* BMDMs (Two-Way ANOVA,  $n = 4$ ). Each flow cytometry trace is representative of at least three separate experiments. The FACS histograms in A–D show the results of one single representative experiment presented in different combinations, as indicated.

*Adam17 $\Delta$ cyto* mice resemble other mice with hypomorphic mutations in the ADAM17/EGFR pathways (16, 44, 45). The ability of female *Adam17 $\Delta$ cyto* mice to give birth and nurse their offspring suggests that reproductive functions and lactation, both of which are known to involve EGFR signaling and ADAM17-dependent processing of the EGFR ligand Amphiregulin (13, 62, 63), are not strongly affected.

Previous studies have shown that pro-ADAM17 is synthesized and retained in the ER in the absence of iRhom1 and 2, with no apparent effect on the stability of pro-ADAM17 (64, 65). The mutant ADAM17 $\Delta$ cyto protein was significantly less stable than the wild-type control in cycloheximide chase experiments in mEFs, demonstrating that the cytoplasmic domain of ADAM17 has an important role in regulating its stability and turnover at the protein level. The low levels of pro- and mature ADAM17 $\Delta$ cyto raise the possibility

that a putative and yet-to-be identified stability factor binds the ADAM17 cytoplasmic domain to stabilize this protein until it can interact with an iRhom protein. Binding of an iRhom to ADAM17 in the ER would then initiate the maturation and trafficking of ADAM17 to the cell surface. A previous study showed that hardly any iRhom2 can be detected in the absence of ADAM17, whereas the levels of iRhom1 were slightly increased (50). Similar results were obtained in a western blot analysis of *Adam17 $\Delta$ cyto* mEFs, which had very little iRhom2 but slightly increased levels of iRhom1, as well as in *Adam17 $\Delta$ cyto* BMDM, which had very little iRhom2, providing additional corroboration that iRhom2 is stabilized by the presence of ADAM17. The levels of ADAM17 $\Delta$ cyto in mEFs were not strongly affected by treatment with inhibitors of proteasomal, lysosomal, or ER-associated degradation pathways, suggesting that these

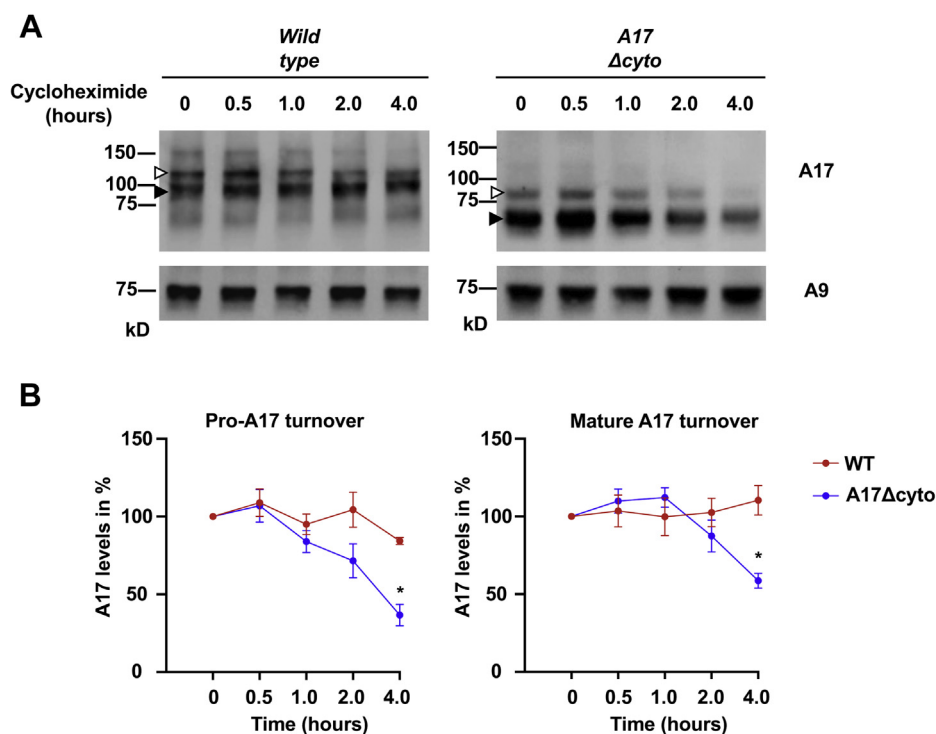


**Figure 10. Cycloheximide chase experiment of wild-type ADAM17 and the ADAM17 $\Delta$ cyto mutant in mEFs.** mEFs from *wild-type* or *Adam17 $\Delta$ cyto* mice were subjected to 100  $\mu$ g/ml cycloheximide treatment (CHX) and chased for 4 h to compare how this affects the levels of wild-type ADAM17 and mutant ADAM17 $\Delta$ cyto protein at different time points (0', 30', 1 h, 2 h, 4 h). *A*, western blot analysis demonstrated that the levels of pro- and mature wild-type ADAM17 are not significantly affected under these conditions (*left panels*), whereas both the pro- and mature forms of ADAM17 $\Delta$ cyto show slightly reduced levels after 2 h CHX treatment and strongly reduced levels after 4 h in CHX. *Open arrowheads*, proform, *black arrowheads*, mature form of ADAM17, or ADAM17 $\Delta$ cyto. The western blot of ADAM17 $\Delta$ cyto was exposed longer than the blot of wild-type ADAM17 to allow a better comparison of the relative levels at different time points compared with untreated cells, with ADAM9 serving as a loading control (*lower panel*). *B*, densitometric analysis of the results of four separate experiments with NIH Image-J corroborated a significant decrease in pro- and mature ADAM17 $\Delta$ cyto compared with the *wild-type* control after 4 h in CHX. The graphs are based on four separate experiments, the 0 h time point is set to 100% for each experiment, and each data point represents the ADAM17 levels in percent relative to the 0 h time point for the proform or the mature form of ADAM17 or ADAM17 $\Delta$ cyto. To test for differences between *wild-type* and *Adam17 $\Delta$ cyto* at different time points, we performed an unpaired Student's *t*-test with Welch correction and post hoc Bonferroni–Dunn correction for multiple hypothesis testing. \* indicates an adjusted *p*-value of <0.05.

pathways do not play a major role in causing the reduced levels of ADAM17 $\Delta$ cyto.

Taken together, these findings are the first to identify a role of the cytoplasmic domain of ADAM17 in stabilizing the levels of this protein. Moreover, they confirm that the cytoplasmic domain of endogenous ADAM17 is not required for its rapid activation by PMA. The reduced levels of ADAM17 are sufficient to support survival of the *ADAM17 $\Delta$ cyto* mice, although they have several ADAM17/EGFR-dependent developmental defects, such as open eyes at birth and heart valve defects, demonstrating that the normal development of these structures requires higher or more physiological activity of ADAM17. Further studies will be necessary to understand the mechanism underlying the regulation of ADAM17 levels by its cytoplasmic domain.

## Experimental procedures

### Reagents and antibodies

Unless otherwise noted, all reagents were purchased from Sigma-Aldrich. The rabbit polyclonal antibody against the ectodomain of ADAM17 was generated by injecting a purified Fc fusion protein with the extracellular domain of human ADAM17 into New Zealand White rabbits (Covance). The

rabbit polyclonal antibodies against ADAM9 and the rat monoclonal antibodies against iRhom1 and iRhom2 have been previously described (50, 66). The antibodies against alpha-tubulin were from Cell Signaling, (Cat. #: 2144). The antibody against LC3 was from Novus Biological (Cat. #: Nb.100-2220), and the anti-ubiquitin antibody was from Biogen (Cat. # 838703). The cell surface biotin reagent EZ Link Sulfo-NHS-LC-Biotin was from Thermo Fisher Scientific (Cat. # 21335), as were the Streptavidin-Sepharose beads (Cat. #: 434341). The metalloprotease inhibitor marimastat was kindly provided by Dr Ouathek Ouerfelli, Memorial Sloan Kettering Cancer Center, New York, NY (67). Cycloheximide was obtained from Cell Signaling (Cat. #: 2112S). The inhibitors of proteasomal degradation, ER-associated degradation (ERAD), and lysosomal degradation were from Sigma-Aldrich: MG-132 (Cat. #: 474790), eeyarestatin (Cat. #: E1286), bafilomycin (Cat. #: B1793), and chloroquine (Cat. #: C6628).

### Mouse lines

The *Adam17 $^{-/-}$*  and *iRhom2 $^{-/-}$*  mice used in this study have been described previously (46, 48). To generate the *Adam17 $\Delta$ cyto* mice, a KI mutation was introduced by targeting

## ADAM17 levels depend on its cytoplasmic domain in mice

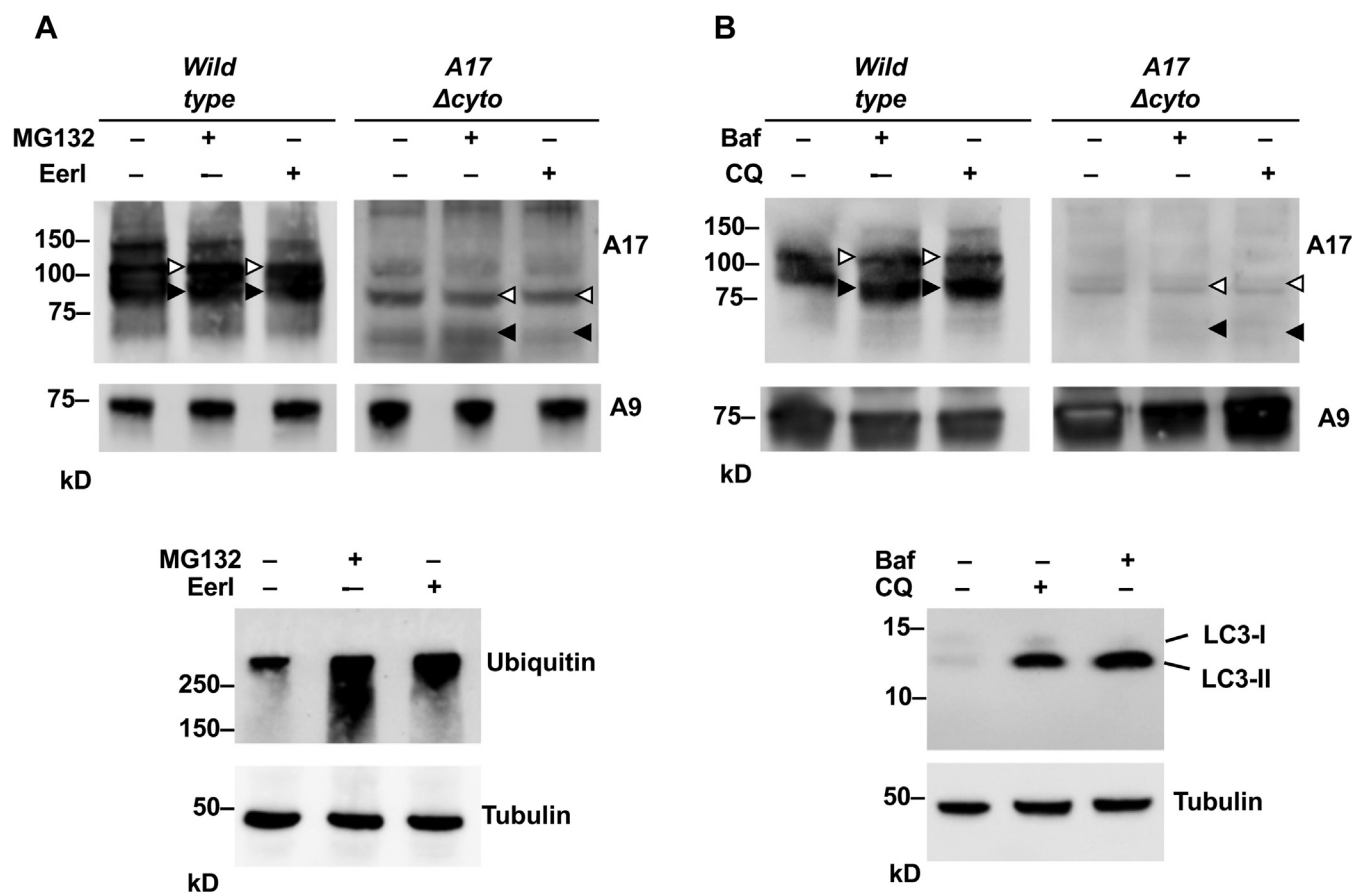


**Figure 11. Effect of inhibitors of proteasomal, lysosomal, and ER-associated degradation on ADAM17 levels in wild-type and *Adam17Δcyto* cells.** Wild-type or *Adam17Δcyto* mEFs were either treated with 10  $\mu$ M of the proteasomal inhibitor MG-132 or the ER-associated degradation (ERAD) inhibitor Eeyarestatin I (Eerl) for 6 h or left untreated before lysis (A). Concanavalin A-enriched protein extracts were subjected to western blot analysis for either ADAM17 or ADAM9 as a loading control (A). As a control for the activity of these inhibitors, lysates of *Adam17Δcyto* mEFs treated under identical conditions were subjected to western blot analysis for Ubiquitin, which corroborated the increased levels caused by a block of proteasomal degradation for MG-132 or of ERAD, with a blot for tubulin serving as a loading control (lower panels). In addition, wild-type or *Adam17Δcyto* mEFs were treated with 100 nM Bafilomycin (BAF) or 100  $\mu$ M Chloroquine (CQ) for 18 h or left untreated and then lysed and prepared for western blot analysis for ADAM17 or ADAM9 as a loading control (B). The activity of inhibitors of lysosomal degradation was confirmed in western blots of extracts of *Adam17Δcyto* mEFs treated with Baf or CQ that were probed with antibodies against LC3-II, which accumulates upon inhibition of the lysosomal degradation pathway (lower panels). Please note that 10% Bis-Tris NuPage gels were used to separate the samples for the western blots shown for ubiquitin, LC3, and the tubulin controls in the lower panels and for the A9 control in A. The results are representative of three independent experiments with essentially similar findings.

the endogenous *Adam17* locus via CRISPR-Cas9 KI mutagenesis.

### Construction of the *Adam17Δcyto* donor vector (DV)

The KI donor shown in Fig. S1B consists of an HA-tag with a stop codon flanked by 5'-homology sequence (514 bp) and 3'-homology sequence (587 bp) to the genomic target. The template was generated by PCR amplifications of two DNA segments from C57Bl/6J-TyrC-2J mouse genomic DNA using two pairs of primers that carry the sequences of HA-tag, stop codon, and BsaI restriction enzyme (RE) sites (see Table S1 in supporting information for details), followed by ligating the PCR products with a pFUS vector backbone via the Golden Gate cloning method (68). Additionally, the seed sequence of the CRISPR target site on the DV was mutagenized with primer Mut-F using QuickChange II (Agilent; Cat. #: 200521) to avoid recleavage of the repaired sequence post KI.

### Selection of guide RNA

We identified a CRISPR target site (CCTATGCTTTC-TAGGATAAGAAA; Fig. S1A, red scissors) at the junction of intron 17 and exon 18 for its optimal proximity to the DV insertion site, albeit with low off-target score. In order to mitigate off-target effects, a shorter version of single guide RNA (sgRNA) carrying only 17 nucleotides sequence upstream of the PAM (CTTATCCTAGAAAGCAT) was hence chosen (69) and was cloned into the pX330 vector (Addgene, plasmid # 42230; a SpCas9 and sgRNA expressing plasmid) following the protocol as described (70). The selected gRNA showed modest cleavage efficiency assessed in mouse embryonic stem (mES) cells.

### Gene editing in mES cells

The DV (7  $\mu$ g) and sgRNA+Cas9 expressing pX330 vector (2  $\mu$ g) were transfected into C57Bl/6J-TyrC-2J mES cells (3  $\times$

10<sup>6</sup> cells) using Lipofectamine 2000 reagent (Thermo Fisher; Cat #: 11668019) with a modified transfection procedure for cell suspensions. Transfected ES cells were plated on mEF feeder cells at low density to obtain single colonies without selection, and individual ES colonies were isolated after 5 days of culture. Genomic DNA from the single colonies were screened *via* PCR using the external primer pair ScrA17-F and ScrA17-R, which amplified 1264 bp for the KI allele *versus* 1234 bp for the *wild-type* allele. The HA-tag carries a BmgBI site, which upon digestion cleaved the 1264 bp KI mutant into two fragments (659 bp and 605 bp), whereas the 1234 bp wild-type fragment was unaffected (Fig. S1C). The PCR product from the positive clone was identified through TOPO cloning as a mixed population, hence each colony was subjected to an additional round of clonal isolation, followed by PCR screening and Sanger sequencing validation. The edited ES cells were microinjected into C57Bl/6J blastocyst and implanted into pseudo-pregnant females. Chimera progeny was obtained and high degree chimeras were mated with C57Bl/6J-TyrC-2J mice to identify germline transmission of the *Adam17 $\Delta$ cyto* allele.

All animal experiments were approved by the Institutional Animal Care and Use Committee of the Hospital for Special Surgery and Weill Cornell Medicine.

### Necropsy and histopathology

The histopathological analysis of adult mice was performed on three pairs of mice from independent litters on a mixed 129SvJ/C57Bl/6J-TyrC-2J genetic background, each pair consisting of one *Adam17 $\Delta$ cyto* mutant and one *wild-type* littermate control. Two pairs were females and one pair was male. All mice were approximately 6.5 weeks old.

Mice were euthanized with CO<sub>2</sub>. Following gross examination, all organs were fixed in 10% neutral buffered formalin, followed by decalcification of bone in a formic acid solution (Surgipath Decalcifier I, Leica Biosystems). Tissues were then processed in ethanol and xylene and embedded in paraffin in a Leica ASP6025 tissue processor. Paraffin blocks were sectioned at 5 microns, stained with hematoxylin and eosin (H&E), and examined by a board-certified veterinary pathologist. The following tissues were processed and examined: the heart, thymus, lungs, liver, gallbladder, kidneys, pancreas, stomach, duodenum, jejunum, ileum, cecum, colon, lymph nodes (submandibular, mesenteric), salivary glands, skin (trunk and head), urinary bladder, uterus, cervix, vagina, ovaries, oviducts, adrenal glands, spleen, thyroid gland, esophagus, trachea, spinal cord, vertebrae, sternum, femur, tibia, stifle joint, skeletal muscle, nerves, skull, nasal cavity, oral cavity, teeth, ears, eyes, pituitary gland, brain.

### Hematology

For hematology, blood was collected into tubes containing EDTA. Automated analysis was performed on an IDEXX Procyte DX hematology analyzer and the following parameters were determined: white blood cell count, red blood cell count, hemoglobin concentration, hematocrit, mean corpuscular volume, mean corpuscular hemoglobin, mean corpuscular hemoglobin concentration, red blood cell distribution width

standard deviation and coefficient of variance, reticulocyte relative and absolute counts, platelet count, platelet distribution width, mean platelet volume, and relative and absolute counts of neutrophils, lymphocytes, monocytes, eosinophils, and basophils.

### Serum chemistry

For serum chemistry, blood was collected into tubes containing a serum separator, the tubes were centrifuged, and the serum was obtained for analysis. Serum chemistry was performed on a Beckman Coulter AU680 analyzer and the concentration of the following analytes was determined: alkaline phosphatase, alanine aminotransferase, aspartate aminotransferase, creatine kinase, gamma-glutamyl transpeptidase, albumin, total protein, globulin, total bilirubin, blood urea nitrogen, creatinine, cholesterol, triglycerides, glucose, calcium, phosphorus, chloride, potassium, and sodium. Finally, the Na/K ratio and albumin/globulin ratio were calculated.

### Isolation and immortalization of mouse embryonic fibroblasts

mEFs were isolated from E13.5 *Adam17 $\Delta$ cyto* embryos to generate primary mEFs as previously described (9, 71). Primary mEFs were immortalized by transduction with a retroviral plasmid carrying the simian virus 40 (SV40) large T antigen and a zeocin resistance cassette. The cell lines used in these studies were routinely genotyped by PCR to corroborate their identity.

### Western blot analysis

To generate western blots for ADAM9, ADAM17, and alpha tubulin with tissue extracts from adult mice, we harvested the brain, heart, lung, liver, and spleen samples from adult mice and processed the samples as previously described (66). Unless otherwise noted, all tissue and cell extracts were lysed on ice or at 4°C in phosphate-buffered saline (PBS) with 1% Triton-X 100, 5  $\mu$ M Marimastat, 10 mM 1,10 Phenanthroline, and protease inhibitor cocktail (1:250) (48). For the ADAM17 and ADAM9 blots, it was crucial that the tissue or cell extract was subjected to Concanavalin A sepharose beads for glycoprotein enrichment (48). Comparable amounts of protein were separated under nonreducing conditions on 10% SDS-PAGE Tris-Glycine gels or on 10% Bis-Tris NuPage gels (Thermo Fisher Scientific, Cat#: NP0301), as indicated, and immobilized onto nitrocellulose membranes (Pall Corp, Cat. #: VMR 27376-991). After blocking in PBS, 0.05% Tween 20, and 5% nonfat dry milk for 1 h at room temperature, the nitrocellulose membrane was incubated overnight at 4 degrees with rabbit polyclonal antibodies raised against an Fc-fusion protein with the extracellular domain of ADAM17 that only recognizes nonreduced ADAM17. The membranes were then washed three times with PBS, 0.05% Tween 20, and incubated in HRP-conjugated goat anti-rabbit secondary (Promega). ADAM9 and alpha-tubulin were used as loading controls by running duplicate gels or by stripping the membranes for 15 min at 55°C in stripping buffer (2% SDS, 50 mM beta-mercaptoethanol in 62 mM Tris, pH 6.7). These membranes were blocked as described above, then incubated with anti-ADAM9 or anti-alpha-tubulin antibodies. Western blots for iRhom1, iRhom2, ubiquitin, and

## ADAM17 levels depend on its cytoplasmic domain in mice

LC3 were performed on samples that were not enriched with Concanavalin A, as described previously (50).

### Biotinylation of cell surface proteins

Cell surface proteins of mEFs were labeled with 1 mg/ml of the membrane impermeable biotinylation reagent EZ-Link Sulfo-NHS-LC-Biotin (Thermo Fisher Scientific) following the manufacturer's protocol. The cells were lysed in PBS, 1% Triton X-100 containing protease inhibitors including the metalloprotease inhibitors 1,10-phenanthroline (10 mM), and marimastat (5  $\mu$ M). The biotinylated fraction of the lysate was pulled down with streptavidin-Sepharose 4B beads for 30 min at 4°C. The beads were washed four times with lysis buffer, and the bound material was eluted in SDS-containing sample loading buffer. The resulting material was then separated on a 10% SDS-PAGE gel and subjected to western blot analysis for ADAM17 or ADAM9 as described above. The ratio of cell surface biotinylated mature ADAM17 to total ADAM17 protein detected by western blot was determined from densitometric quantification of the bands by NIH Image J, normalized using ADAM9 as a loading control.

### Flow cytometry staining and ADAM17 MFI quantification

The skin was prepared for flow cytometry as previously described (72, 73). Murine ear skin was excised and finely minced and digested with dispase (Thermo Fisher Scientific), type II collagenase (Worthington) and DNaseI (Sigma Aldrich). Cells were then triturated with Pasteur pipettes and further incubated with EDTA before being passed through a 70  $\mu$ m nylon filter to generate a single cell suspension used for flow cytometric staining.

Skin cells were stained with Fc-block (Biolegend) followed by anti-CD45 anti-EpCAM (all Biolegend) and anti-ADAM17. Donkey anti-rabbit IgG (Jackson Immunoresearch) was used to detect the anti-ADAM17. 4',6-diamidino-2-phenylindole dihydrochloride (DAPI) was used to exclude dead cells and debris (Sigma Aldrich). Normal rabbit serum (Jackson Immunoresearch) was used as a negative control for ADAM17.

For ADAM17 mean fluorescence intensity (MFI) quantification, all ADAM17 MFIs were normalized to the wild-type control in the same experiment.

### TGF $\alpha$ ectodomain shedding assay

*Wild-type*, *Adam17 $\Delta$ cyto*, and *Adam17 $^{-/-}$*  mEFs were transfected with alkaline phosphatase-tagged TGF $\alpha$  using Lipofectamine 2000, following the manufacturer's instructions (Thermo Fisher, Cat. # 12566014). On the following day, the cells were incubated in Opti-MEM (Gibco) for 30 min and then fresh Opti-MEM was added for 45 min with or without the addition of 25 ng/ml phorbol 12-myristate 13-acetate (PMA) to stimulate ADAM17-dependent shedding, in the presence or absence of 5  $\mu$ M marimastat. The supernatants were collected and the cells were lysed as described above. To measure the alkaline phosphatase activity in the cell supernatants and lysates, we added the alkaline phosphatase substrate para-nitrophenyl phosphate and measured the optical density at  $A_{405\text{nm}}$ . The optical density was

determined for three identical technical replicates, and the data shown represents three independent trials.

### Isolation of mouse primary bone-marrow-derived macrophages (BMDMs) and Csf1r flow cytometry

To generate primary BMDMs, we isolated bone marrows from adult mice (6 weeks or older with at least a 2:1 sex ratio distribution) as previously described (50). Bone marrow from femurs and tibiae was washed with PBS and passed through a 70  $\mu$ m cell strainer (Denville Scientific) before plating on Petri dishes in DMEM supplemented with 20% fetal calf serum and 10 ng/ml of murine macrophage-colony stimulating factor (Peprotech, Cat. #: 315-02). After 7 days, macrophages were removed with Accutase (Sigma-Aldrich, Cat#: A6964), plated on tissue culture plates, and left untreated or treated with 25 ng/ml PMA for 45 min on the following day. BMDMs were lysed and subjected to western blot analysis for ADAM17 and alpha tubulin or the cell surface levels of the Csf1R were measured by flow cytometry with anti-CD115 antibodies (Biolegend, Clone: AFS98).

### qRT-PCR analysis

#### Tissues

Total RNA was isolated from the tissues (the brain, heart, lung, liver, spleen) of adult mice that were at least 6 weeks old using TRIzol reagent (Thermo Fisher Scientific). The resulting material was subjected to a standard ethanol/sodium acetate precipitation protocol for nucleic acids to remove salts and impurities and then used for reverse transcription, as outlined below.

#### Bone-marrow-derived macrophages

BMDMs were isolated as described above and differentiated for 7 days, at which point their RNA was isolated using the RNeasy mini kit from Qiagen.

Total RNA was reverse-transcribed using RNasin Plus (Promega), 2.5 mM dNTPs, Random Primer 9, and M-MuLV Reverse Transcriptase from NEB. ADAM17 oligonucleotides were purchased from Eurofins Genomics using previously described sequences (72), ADAM17 Forward 5'-GATGCT-GAAGATGACACTGTG-3' (A17 exon 14); ADAM17 Reverse 5'-GAGTTGTCAGTGTCAACGC-3' (ADAM17 exon 14–15). GAPDH oligonucleotides were purchased from Qiagen. ADAM17 mRNA in *wild-type* and *Adam17 $\Delta$ cyto* tissues was quantified *via* RT-qPCR using SYBR Green Reagent and an ABI PRISM 7900HT cyler (both from Applied Biosystems, Thermo Fisher Scientific). GAPDH was used as a housekeeping control. Three independent experiments were performed with duplicate or triplicate samples for each experiment.

### TNF $\alpha$ ELISA

Primary BMDMs differentiated for 7 days (see above) were harvested using Accutase solution and re-plated at  $1.25 \times 10^5$  cells/well in 0.4 ml complete DMEM in a 24-well format. On the following day, BMDMs were treated with 2.0  $\mu$ g/ml Lipopolysaccharide (LPS) for 3 h to stimulate production and shedding of TNF $\alpha$  or left untreated. After 3 h, the culture supernatants were collected to measure the amount of soluble

released TNF $\alpha$  by ELISA with a kit specific for murine TNF $\alpha$  (Duoset ELISA DY410, R&D Systems).

### Cycloheximide chase assay and protein degradation inhibitors

*Wild-type* and *Adam17 $\Delta$ cyto* mEFs were plated in a 6-well format and grown to 90 to 100% confluency. Cells were then treated with 100  $\mu$ g/ml cycloheximide in freshly prepared complete DMEM (10% FCS, 1% P/S) supplemented with 15 mM HEPES and lysed at the corresponding time points – 0 h, 0.5 h, 1 h, 2 h, and 4 h, as described above. The samples were enriched for glycoproteins using Concanavalin A sepharose beads and used for western blot analysis of ADAM17, with western blots of ADAM9 serving as loading control. The band intensities of wild-type ADAM17 and ADAM17 $\Delta$ cyto at each time point were determined *via* densitometry in ImageJ and used to calculate the percentage remaining at each time point compared with the levels at 0 h.

In western blot experiments with protein degradation inhibitors, the inhibitors were used at the following concentrations and time points: MG-132 and eeyarestatin at 10  $\mu$ M for 6 h; Bafilomycin at 100 nM and chloroquine at 100  $\mu$ M, both for 18 h (30, 31, 74).

### Statistical analysis

All graphs are presented as mean  $\pm$  SEM and were analyzed with GraphPad Prism 8.4.3. To calculate the statistical significance, we proceeded as follows. An unpaired two-tailed Student's *t*-test was used for the qRT-PCR results, AP-TGF $\alpha$  shedding assays, and ADAM17 MFI from flow cytometry experiments in Figures 5–7. A two-way ANOVA was used for the TNF $\alpha$  ELISA shown in Figure 9E. A Welch unpaired Student's *t*-test and post hoc Bonferroni–Dunn correction for multiple hypothesis correction was used for the cycloheximide chase assay in Figure 10.

In all cases, a *p*-value or corrected *p*-value of  $<0.05$  was considered statistically significant (indicated by \*).

### Data availability

All the data described in this article are contained within the article.

**Supporting information**—This article contains supporting information.

**Acknowledgments**—We thank Daniel Li for excellent technical assistance.

**Author contributions**—J. L., G. W., and C. P. B. conceived the study; J. L., G. W., T. M. L., T. M., D. T. N. S., S. M., and C. Y. designed and performed the experiments and analyzed the data; S. F. L. provided key reagents and intellectual input; J. L. and C. P. B. wrote the article; all the authors contributed to editing and article revisions.

**Funding and additional information**—J. L. is supported by NIH F31 GM136144 and was previously supported by T32 GM008539. S. M. and the Laboratory of Comparative Pathology are supported in part

by Cancer Center Support Grant P30CA008748. D. T. N. S. and C. Y. are supported by The Rockefeller University through the CRISPR & Genome Editing Resource Center. This work was also funded by the Deutsche Forschungsgemeinschaft (DFG, German Research Foundation) under Germany's Excellence Strategy within the framework of the Munich Cluster for Systems Neurology (EXC 2145 SyNergy- ID 390857198). Support for this project was provided by NIH R35 GM134907 to C. P. B. The content is solely the responsibility of the authors and does not necessarily represent the official views of the National Institutes of Health.

**Conflict of interest**—Drs Maretzky and Blobel hold a patent on a method of identifying agents for combination with inhibitors of iRhoms. Dr Blobel and the Hospital for Special Surgery have identified iRhom2 inhibitors and have cofounded the start-up company SciRhom in Munich to commercialize these inhibitors.

**Abbreviations**—The abbreviations used are: ADAM17, a disintegrin and metalloprotease 17; BMDM, bone-marrow-derived macrophage; CHX, cycloheximide; DV, donor vector; EGFR, epidermal growth factor receptor; EPCAM, epithelial cell adhesion molecule; IL-6R, interleukin-6 receptor; iRhom1 and 2, inactive Rhomboid proteins 1 and 2; KI, knock-in; mEF, mouse embryonic fibroblast; mES, mouse embryonic stem; MFI, mean fluorescence intensity; PMA, phorbol 12-myristate 13-acetate; TNF $\alpha$ , tumor necrosis factor  $\alpha$ .

### References

- Murphy, G. (2008) The ADAMs: Signalling scissors in the tumour microenvironment. *Nat. Rev. Cancer* **12**, 929–941
- Weber, S., and Saftig, P. (2012) Ectodomain shedding and ADAMs in development. *Development* **139**, 3693–3709
- Blobel, C. P. (2005) ADAMs: Key players in EGFR-signaling, development and disease. *Nat. Rev. Mol. Cell. Biol.* **6**, 32–43
- Zunke, F., and Rose-John, S. (2017) The shedding protease ADAM17: Physiology and pathophysiology. *Biochim. Biophys. Acta Mol. Cell Res.* **1864**, 2059–2070
- Black, R., Rauch, C. T., Kozlosky, C. J., Peschon, J. J., Slack, J. L., Wolfson, M. F., Castner, B. J., Stocking, K. L., Reddy, P., Srinivasan, S., Nelson, N., Boiani, N., Schooley, K. A., Gerhart, M., Davis, R., *et al.* (1997) A metalloprotease disintegrin that releases tumour-necrosis factor- $\alpha$  from cells. *Nature* **385**, 729–733
- Moss, M. L., Jin, S.-L. C., Milla, M. E., Burkhart, W., Cartner, H. L., Chen, W.-J., Clay, W. C., Didsbury, J. R., Hassler, D., Hoffman, C. R., Kost, T. A., Lambert, M. H., Lessnitzer, M. A., McCauley, P., McGeehan, G., *et al.* (1997) Cloning of a disintegrin metalloproteinase that processes precursor tumour-necrosis factor- $\alpha$ . *Nature* **385**, 733–736
- Peschon, J. J., Slack, J. L., Reddy, P., Stocking, K. L., Sunnarborg, S. W., Lee, D. C., Russel, W. E., Castner, B. J., Johnson, R. S., Fitzner, J. N., Boyce, R. W., Nelson, N., Kozlosky, C. J., Wolfson, M. F., Rauch, C. T., *et al.* (1998) An essential role for ectodomain shedding in mammalian development. *Science* **282**, 1281–1284
- Sunnarborg, S. W., Hinkle, C. L., Stevenson, M., Russell, W. E., Raska, C. S., Peschon, J. J., Castner, B. J., Gerhart, M. J., Paxton, R. J., Black, R. A., and Lee, D. C. (2002) Tumor necrosis factor- $\alpha$  converting enzyme (TACE) regulates epidermal growth factor receptor ligand availability. *J. Biol. Chem.* **277**, 12838–12845
- Sahin, U., Weskamp, G., Zhou, H. M., Higashiyama, S., Peschon, J. J., Hartmann, D., Saftig, P., and Blobel, C. P. (2004) Distinct roles for ADAM10 and ADAM17 in ectodomain shedding of six EGFR-ligands. *J. Cell Biol.* **164**, 769–779
- Garbers, C., Heink, S., Korn, T., and Rose-John, S. (2018) Interleukin-6: Designing specific therapeutics for a complex cytokine. *Nat. Rev. Drug Discov.* **17**, 395–412

## ADAM17 levels depend on its cytoplasmic domain in mice

- Rose-John, S. (2017) The soluble interleukin 6 receptor: Advanced therapeutic options in inflammation. *Clin. Pharmacol. Ther.* **102**, 591–598
- Jackson, L. F., Qiu, T. H., Sunnarborg, S. W., Chang, A., Zhang, C., Patterson, C., and Lee, D. C. (2003) Defective valvulogenesis in HB-EGF and TACE-null mice is associated with aberrant BMP signaling. *EMBO J.* **22**, 2704–2716
- Sternlicht, M. D., Sunnarborg, S. W., Kouros-Mehr, H., Yu, Y., Lee, D. C., and Werb, Z. (2005) Mammary ductal morphogenesis requires paracrine activation of stromal EGFR via ADAM17-dependent shedding of epithelial amphiregulin. *Development* **132**, 3923–3933
- Hall, K. C., Hill, D., Otero, M., Plumb, D. A., Froemel, D., Dragomir, C. L., Maretzky, T., Boskey, A., Crawford, H. C., Selleri, L., Goldring, M. B., and Blobel, C. P. (2013) ADAM17 controls endochondral ossification by regulating terminal differentiation of chondrocytes. *Mol. Cell. Biol.* **33**, 3077–3090
- Saito, K., Horiuchi, K., Kimura, T., Mizuno, S., Yoda, M., Morioka, H., Akiyama, H., Threadgill, D., Okada, Y., Toyama, Y., and Sato, K. (2013) Conditional inactivation of TNF $\alpha$ -converting enzyme in chondrocytes results in an elongated growth plate and shorter long bones. *PLoS One* **8**, e54853
- Chalaris, A., Adam, N., Sina, C., Rosenstiel, P., Lehmann-Koch, J., Schirmacher, P., Hartmann, D., Cichy, J., Gavrilova, O., Schreiber, S., Jostock, T., Mathews, V., Hasler, R., Becker, C., Neurath, M. F., et al. (2010) Critical role of the disintegrin metalloprotease ADAM17 for intestinal inflammation and regeneration in mice. *J. Exp. Med.* **207**, 1617–1624
- Franzke, C. W., Cobzaru, C., Triantafyllidou, A., Loffek, S., Horiuchi, K., Threadgill, D. W., Kurz, T., van Rooijen, N., Bruckner-Tuderman, L., and Blobel, C. P. (2012) Epidermal ADAM17 maintains the skin barrier by regulating EGFR ligand-dependent terminal keratinocyte differentiation. *J. Exp. Med.* **209**, 1105–1119
- Blaydon, D. C., Biancheri, P., Di, W. L., Plagnol, V., Cabral, R. M., Brooke, M. A., van Heel, D. A., Ruschendorf, F., Toynbee, M., Walne, A., O'Toole, E. A., Martin, J. E., Lindley, K., Vulliamy, T., Abrams, D. J., et al. (2011) Inflammatory skin and bowel disease linked to ADAM17 deletion. *N. Engl. J. Med.* **365**, 1502–1508
- Ardito, C. M., Gruner, B. M., Takeuchi, K. K., Lubeseder-Martellato, C., Teichmann, N., Mazur, P. K., Delgiorno, K. E., Carpenter, E. S., Halbrook, C. J., Hall, J. C., Pal, D., Briel, T., Herner, A., Trajkovic-Arsic, M., Sipos, B., et al. (2012) EGF receptor is required for KRAS-induced pancreatic tumorigenesis. *Cancer Cell* **22**, 304–317
- Saad, M. I., Alhayyani, S., McLeod, L., Yu, L., Alanazi, M., Deswaerte, V., Tang, K., Jarde, T., Smith, J. A., Prodanovic, Z., Tate, M. D., Balic, J. J., Watkins, D. N., Cain, J. E., Bozinovski, S., et al. (2019) ADAM17 selectively activates the IL-6 trans-signaling/ERK MAPK axis in KRAS-addicted lung cancer. *EMBO Mol. Med.* **11**, e9976
- Weskamp, G., Mendelson, K., Swendeman, S., Le Gall, S., Ma, Y., Lyman, S., Hinoki, A., Eguchi, S., Guaquil, V., Horiuchi, K., and Blobel, C. P. (2010) Pathological neovascularization is reduced by inactivation of ADAM17 in endothelial cells but not in pericytes. *Circ. Res.* **106**, 932–940
- Issuree, P. D., Maretzky, T., McIlwain, D. R., Monette, S., Qing, X., Lang, P. A., Swendeman, S. L., Park-Min, K. H., Binder, N., Kalliolias, G. D., Yafilina, A., Horiuchi, K., Ivashkiv, L. B., Mak, T. W., Salmon, J. E., et al. (2013) iRHOM2 is a critical pathogenic mediator of inflammatory arthritis. *J. Clin. Invest.* **123**, 928–932
- Qing, X., Chinenov, Y., Redecha, P., Madaio, M., Roelofs, J. J., Farber, G., Issuree, P. D., Donlin, L., McIlwain, D. R., Mak, T. W., Blobel, C. P., and Salmon, J. E. (2018) iRhom2 promotes lupus nephritis through TNF $\alpha$  and EGFR signaling. *J. Clin. Invest.* **128**, 1397–1412
- Reddy, P., Slack, J. L., Davis, R., Cerretti, D. P., Kozlosky, C. J., Blanton, R. A., Shows, D., Peschon, J. J., and Black, R. A. (2000) Functional analysis of the domain structure of tumor necrosis factor- $\alpha$  converting enzyme. *J. Biol. Chem.* **275**, 14608–14614
- Hall, K., and Blobel, C. P. (2012) Interleukin-1 stimulates ADAM17 through a mechanism independent of its cytoplasmic domain or phosphorylation at threonine 735. *PLoS One* **7**, e31600
- Schwarz, J., Broder, C., Helmstetter, A., Schmidt, S., Yan, I., Muller, M., Schmidt-Arras, D., Becker-Pauly, C., Koch-Nolte, F., Mittrucker, H. W., Rabe, B., Rose-John, S., and Chalaris, A. (2013) Short-term TNF $\alpha$  shedding is independent of cytoplasmic phosphorylation or furin cleavage of ADAM17. *Biochim. Biophys. Acta* **1833**, 3355–3367
- Le Gall, S. M., Maretzky, T., Issuree, P. D. A., Niu, X.-D., Reiss, K., Saftig, P., Khokha, R., Lundell, D., and Blobel, C. P. (2010) ADAM17 is regulated by a rapid and reversible mechanism that controls access to its catalytic site. *J. Cell Sci.* **123**, 3913–3922
- Maretzky, T., Evers, A., Zhou, W., Swendeman, S. L., Wong, P. M., Rafii, S., Reiss, K., and Blobel, C. P. (2011) Migration of growth factor-stimulated epithelial and endothelial cells depends on EGFR transactivation by ADAM17. *Nat. Commun.* **2**, 229
- Grieve, A. G., Xu, H., Kunzel, U., Bambrough, P., Sieber, B., and Freeman, M. (2017) Phosphorylation of iRhom2 at the plasma membrane controls mammalian TACE-dependent inflammatory and growth factor signalling. *Elife* **6**, e23968
- Kunzel, U., Grieve, A. G., Meng, Y., Sieber, B., Cowley, S. A., and Freeman, M. (2018) FRMD8 promotes inflammatory and growth factor signalling by stabilising the iRhom/ADAM17 sheddase complex. *Elife* **7**, e35012
- Oikonomidi, I., Burbridge, E., Cavadas, M., Sullivan, G., Collis, B., Naegele, H., Clancy, D., Brezinova, J., Hu, T., Bileck, A., Gerner, C., Bolado, A., von Kriegsheim, A., Martin, S. J., Steinberg, F., et al. (2018) iTAP, a novel iRhom interactor, controls TNF secretion by policing the stability of iRhom/TACE. *Elife* **7**, e35032
- Cavadas, M., Oikonomidi, I., Gaspar, C. J., Burbridge, E., Badenes, M., Felix, I., Bolado, A., Hu, T., Bileck, A., Gerner, C., Domingos, P. M., von Kriegsheim, A., and Adrain, C. (2017) Phosphorylation of iRhom2 controls stimulated proteolytic shedding by the metalloprotease ADAM17/TACE. *Cell Rep.* **21**, 745–757
- Diaz-Rodriguez, E., Montero, J. C., Esparis-Ogando, A., Yuste, L., and Pandiella, A. (2002) Extracellular signal-regulated kinase phosphorylates tumor necrosis factor  $\alpha$ -converting enzyme at threonine 735: A potential role in regulated shedding. *Mol. Biol. Cell* **13**, 2031–2044
- Killock, D. J., and Ivetic, A. (2010) The cytoplasmic domains of TNF $\alpha$ -converting enzyme (TACE/ADAM17) and L-selectin are regulated differently by p38 MAPK and PKC to promote ectodomain shedding. *Biochem. J.* **428**, 293–304
- Kruse, T., Gnosa, S. P., Nasa, I., Garvanska, D. H., Hein, J. B., Nguyen, H., Samsøe-Petersen, J., Lopez-Mendez, B., Hertz, E. P. T., Schwarz, J., Pena, H. S., Nikodemus, D., Kveiborg, M., Kettenbach, A. N., and Nilsson, J. (2020) Mechanisms of site-specific dephosphorylation and kinase opposition imposed by PP2A regulatory subunits. *EMBO J.* **39**, e103695
- Peiretti, F., Canault, M., Deprez-Beauchair, P., Berthet, V., Bonardo, B., Juhan-Vague, I., and Nalbone, G. (2003) Intracellular maturation and transport of tumor necrosis factor  $\alpha$  converting enzyme. *Exp. Cell Res.* **285**, 278–285
- Aragao, A. Z., Nogueira, M. L., Granato, D. C., Simabuco, F. M., Honorato, R. V., Hoffman, Z., Yokoo, S., Laurindo, F. R., Squina, F. M., Zeri, A. C., Oliveira, P. S., Sherman, N. E., and Paes Leme, A. F. (2012) Identification of novel interaction between ADAM17 (a disintegrin and metalloprotease 17) and thioredoxin-1. *J. Biol. Chem.* **287**, 43071–43082
- Dombernowsky, S. L., Samsøe-Petersen, J., Petersen, C. H., Instrell, R., Hedegaard, A. M., Thomas, L., Atkins, K. M., Auclair, S., Albrechtsen, R., Mygind, K. J., Frohlich, C., Howell, M., Parker, P., Thomas, G., and Kveiborg, M. (2015) The sorting protein PACS-2 promotes ErbB signalling by regulating recycling of the metalloproteinase ADAM17. *Nat. Commun.* **6**, 7518
- Xu, P., and Derynck, R. (2010) Direct activation of TACE-mediated ectodomain shedding by p38 MAP kinase regulates EGF receptor-dependent cell proliferation. *Mol. Cell* **37**, 551–566
- Xu, P., Liu, J., Sakaki-Yumoto, M., and Derynck, R. (2012) TACE activation by MAPK-mediated regulation of cell surface dimerization and TIMP3 association. *Sci. Signal* **5**, ra34
- Fan, H., Turck, C. W., and Derynck, R. (2003) Characterization of growth factor-induced serine phosphorylation of tumor necrosis factor- $\alpha$  converting enzyme and of an alternatively translated polypeptide. *J. Biol. Chem.* **278**, 18617–18627

42. Soond, S. M., Everson, B., Riches, D. W., and Murphy, G. (2005) ERK-mediated phosphorylation of Thr735 in TNF $\alpha$ -converting enzyme and its potential role in TACE protein trafficking. *J. Cell Sci.* **118**, 2371–2380
43. Dusterhoft, S., Babendreyer, A., Giese, A. A., Flasshove, C., and Ludwig, A. (2019) Status update on iRhom and ADAM17: It's still complicated. *Biochim. Biophys. Acta Mol. Cell Res.* **1866**, 1567–1583
44. Brandl, K., Sun, L., Nepl, C., Siggs, O. M., Le Gall, S. M., Tomisato, W., Li, X., Du, X., Maennel, D. N., Blobel, C. P., and Beutler, B. (2010) MyD88 signaling in nonhematopoietic cells protects mice against induced colitis by regulating specific EGF receptor ligands. *Proc. Natl. Acad. Sci. U. S. A.* **107**, 19967–19972
45. Hassemer, E. L., Le Gall, S. M., Liegel, R., McNally, M., Chang, B., Zeiss, C. J., Dubielzig, R. D., Horiuchi, K., Kimura, T., Okada, Y., Blobel, C. P., and Sidjanin, D. J. (2010) The waved with open eyelids (woe) locus is a hypomorphic mouse mutation in Adam17. *Genetics* **185**, 245–255
46. Horiuchi, K., Kimura, T., Miyamoto, T., Takaishi, H., Okada, Y., Toyama, Y., and Blobel, C. P. (2007) Cutting edge: TNF- $\alpha$ -converting enzyme (TACE/ADAM17) inactivation in mouse myeloid cells prevents lethality from endotoxin shock. *J. Immunol.* **179**, 2686–2689
47. Schlöndorff, J., Becherer, J. D., and Blobel, C. P. (2000) Intracellular maturation and localization of the tumour necrosis factor alpha convertase (TACE). *Biochem. J.* **347 Pt 1**, 131–138
48. McIlwain, D. R., Lang, P. A., Maretzky, T., Hamada, K., Ohishi, K., Maney, S. K., Berger, T., Murthy, A., Duncan, G., Xu, H. C., Lang, K. S., Haussinger, D., Wakeham, A., Itie-Youten, A., Khokha, R., et al. (2012) iRhom2 regulation of TACE controls TNF-mediated protection against *Listeria* and responses to LPS. *Science* **335**, 229–232
49. Brummer, T., Pignoni, M., Rossello, A., Wang, H., Noy, P. J., Tomlinson, M. G., Blobel, C. P., and Lichtenthaler, S. F. (2018) The metalloprotease ADAM10 (a disintegrin and metalloprotease 10) undergoes rapid, postlysis autocatalytic degradation. *FASEB J.* **32**, 3560–3573
50. Weskamp, G., Tushaus, J., Li, D., Feederle, R., Maretzky, T., Swendeman, S., Falck-Pedersen, E., McIlwain, D. R., Mak, T. W., Salmon, J. E., Lichtenthaler, S. F., and Blobel, C. P. (2020) ADAM17 stabilizes its interacting partner inactive Rhomboid 2 (iRhom2) but not inactive Rhomboid 1 (iRhom1). *J. Biol. Chem.* **295**, 4350–4358
51. Becker, A. M., Walcheck, B., and Bhattacharya, D. (2015) ADAM17 limits the expression of CSF1R on murine hematopoietic progenitors. *Exp. Hematol.* **43**, 44–52.e1-3
52. Qing, X., L. D. R., Mortha, A., Lavin, Y., Redecha, P., Issuree, P. D., Maretzky, T., Merad, M., D. R. M., Mak, T. W., Overall, C. M., Blobel, C. P., and Salmon, J. E. (2016) iRhom2 regulates CSF1R cell surface expression and non-steady state myelopoiesis in mice. *Eur. J. Immunol.* **46**, 2737–2748
53. Li, X., Maretzky, T., Perez-Aguilar, J. M., Monette, S., Weskamp, G., Le Gall, S., Beutler, B., Weinstein, H., and Blobel, C. P. (2017) Structural modeling defines transmembrane residues in ADAM17 that are crucial for Rhbdf2/ADAM17-dependent proteolysis. *J. Cell Sci.* **130**, 868–878
54. Adrain, C., Zettl, M., Christova, Y., Taylor, N., and Freeman, M. (2012) Tumor necrosis factor signaling requires iRhom2 to promote trafficking and activation of TACE. *Science* **335**, 225–228
55. Rosendahl, M. S., Ko, S. C., Long, D. L., Brewer, M. T., Rosenzweig, B., Hedl, E., Anderson, L., Pyle, S. M., Moreland, J., Meyers, M. A., Kohno, T., Lyons, D., and Lichenstein, H. S. (1997) Identification and characterization of a pro-tumor necrosis factor- $\alpha$ -processing enzyme from the ADAM family of zinc metalloproteases. *J. Biol. Chem.* **272**, 24588–24593
56. Lunn, C. A., Fan, X., Dalie, B., Miller, K., Zavodny, P. J., Narula, S. K., and Lundell, D. (1997) Purification of ADAM10 from bovine spleen as TNF $\alpha$  convertase. *FEBS Lett.* **400**, 333–335
57. Horiuchi, K., Le Gall, S., Schulte, M., Yamaguchi, T., Reiss, K., Murphy, G., Toyama, Y., Hartmann, D., Saftig, P., and Blobel, C. (2007) Substrate selectivity of EGF-receptor ligand sheddases and their regulation by phorbol esters and calcium influx. *Mol. Biol. Cell* **18**, 176–188
58. Siggs, O. M., Xiao, N., Wang, Y., Shi, H., Tomisato, W., Li, X., Xia, Y., and Beutler, B. (2012) iRhom2 is required for the secretion of mouse TNF $\alpha$ . *Blood* **119**, 5769–5771
59. Tang, B., Li, X., Maretzky, T., Perez-Aguilar, J. M., McIlwain, D., Xie, Y., Zheng, Y., Mak, T. W., Weinstein, H., and Blobel, C. P. (2020) Substrate-selective protein ectodomain shedding by ADAM17 and iRhom2 depends on their juxtamembrane and transmembrane domains. *FASEB J.* **34**, 4956–4969
60. Dong, F., Call, M., Xia, Y., and Kao, W. W. (2017) Role of EGF receptor signaling on morphogenesis of eyelid and meibomian glands. *Exp. Eye Res.* **163**, 58–63
61. Luetteke, N. C., Qiu, T. H., Peiffer, R. L., Oliver, P., Smithies, O., and Lee, D. C. (1993) TGF  $\alpha$  deficiency results in hair follicle and eye abnormalities in targeted and waved-1 mice. *Cell* **73**, 263–278
62. Adamson, E. D. (1990) Developmental activities of the epidermal growth factor receptor. *Curr. Top. Dev. Biol.* **24**, 1–29
63. Shimada, M., Umehara, T., and Hoshino, Y. (2016) Roles of epidermal growth factor (EGF)-like factor in the ovulation process. *Reprod. Med. Biol.* **15**, 201–216
64. Li, X., Maretzky, T., Weskamp, G., Monette, S., Qing, X., Issuree, P. D., Crawford, H. C., McIlwain, D. R., Mak, T. W., Salmon, J. E., and Blobel, C. P. (2015) iRhoms 1 and 2 are essential upstream regulators of ADAM17-dependent EGFR signaling. *Proc. Natl. Acad. Sci. U. S. A.* **112**, 6080–6085
65. Christova, Y., Adrain, C., Bambrough, P., Ibrahim, A., and Freeman, M. (2013) Mammalian iRhoms have distinct physiological functions including an essential role in TACE regulation. *EMBO Rep.* **14**, 884–890
66. Weskamp, G., Krätzschar, J. R., Reid, M., and Blobel, C. P. (1996) MDC9, a widely expressed cellular disintegrin containing cytoplasmic SH3 ligand domains. *J. Cell Biol.* **132**, 717–726
67. Maretzky, T., Yang, G., Ouerfelli, O., Overall, C. M., Worpenberg, S., Hassiepen, U., Eder, J., and Blobel, C. P. (2009) Characterization of the catalytic activity of the membrane-anchored metalloproteinase ADAM15 in cell-based assays. *Biochem. J.* **420**, 105–113
68. Engler, C., Kandzia, R., and Marillonnet, S. (2008) A one pot, one step, precision cloning method with high throughput capability. *PLoS One* **3**, e3647
69. Fu, Y., Sander, J. D., Reyon, D., Cascio, V. M., and Joung, J. K. (2014) Improving CRISPR-Cas nuclease specificity using truncated guide RNAs. *Nat. Biotechnol.* **32**, 279–284
70. Cong, L., Ran, F. A., Cox, D., Lin, S., Barretto, R., Habib, N., Hsu, P. D., Wu, X., Jiang, W., Marraffini, L. A., and Zhang, F. (2013) Multiplex genome engineering using CRISPR/Cas systems. *Science* **339**, 819–823
71. Sahin, U., Weskamp, G., Zheng, Y., Chesneau, V., Horiuchi, K., and Blobel, C. P. (2006) A sensitive method to monitor ectodomain shedding of ligands of the epidermal growth factor receptor. In: Patel, T. B., Bertics, P. J., eds. *Epidermal Growth Factor: Methods and Protocols*, Humana Press Inc, Totowa, NJ: 99–113
72. Chia, J. J., Zhu, T., Chyou, S., Dasoveanu, D. C., Carballo, C., Tian, S., Magro, C. M., Rodeo, S., Spiera, R. F., Ruddle, N. H., McGraw, T. E., Browning, J. L., Lafyatis, R., Gordon, J. K., and Lu, T. T. (2016) Dendritic cells maintain dermal adipose-derived stromal cells in skin fibrosis. *J. Clin. Invest.* **126**, 4331–4345
73. Shipman, W. D., Chyou, S., Ramanathan, A., Izmirly, P. M., Sharma, S., Pannellini, T., Dasoveanu, D. C., Qing, X., Magro, C. M., Granstein, R. D., Lowes, M. A., Pamer, E. G., Kaplan, D. H., Salmon, J. E., Mehrara, B. J., et al. (2018) A protective Langerhans cell-keratinocyte axis that is dysfunctional in photosensitivity. *Sci. Transl. Med.* **10**, eaap9527
74. Wang, Q., Li, L., and Ye, Y. (2008) Inhibition of p97-dependent protein degradation by Eeyarestatin I. *J. Biol. Chem.* **283**, 7445–7454